2017

EVOLUTION OF THE KINETICS AND DYNAMICS OF HEME-CREVICE LOOP REGULATING CHEMISTRY IN HUMAN CYTOCHROME C

Shiloh M. Nold
University of Montana, Missoula

EVOLUTION OF THE KINETICS AND DYNAMICS OF HEME-CREVICE LOOP REGULATING CHEMISTRY IN HUMAN CYTOCHROME *C*

By

SHILOH MICHAELA NOLD

B.S., Biochemistry – Honors Scholar, University of Missouri, Columbia, MO, USA, 2013

Thesis

Presented in partial fulfillment of the requirements for the degree of

Master of Science in Biochemistry and Biophysics

The University of Montana, Missoula, MT

May 2017

Approved by:

Dr. Bruce E. Bowler, Chair
Department of Chemistry & Biochemistry

Dr. J. B. Alexander (Sandy) Ross, Committee Member
Department of Chemistry & Biochemistry

Dr. D. Scott Samuels, Committee Member
Biochemistry Program

Dr. Scott Miller, Committee Member
Division of Biological Science

Nold, Shiloh M., M.S. Spring 2017 Chemistry and Biochemistry

Evolution of the Kinetics and Dynamics of Heme-Crevice Loop Regulating Chemistry in Human Cytochrome *c*

Chairperson: Bruce E. Bowler

Cytochrome *c*, cyt*c*, is a metalloprotein that plays primary roles in electron transport and intrinsic apoptotic pathways. Much of the chemistry that cyt*c* is involved with is regulated by a highly conserved region known as the heme crevice loop, consisting of residues 70-85. Only three of these residues (those at positions 81, 83 and 85) are not universally conserved within the evolutionary timeline. Here I look to elucidate possible evolutionary roles for several of the key residues known to be important in regulating heme chemistry of cyt*c*.

I first address the role that lysine 72 plays in cyt*c* folding and chemistry. Here I provide evidence that K72 alters the alkaline conformational transition of cyt*c*. Trimethylated lysine 72, tmK72, was previously investigated and shows similar trends in peroxidase activity (McClelland et al 2013).

Lastly I address I81 which is not only within the heme crevice loop and not universally conserved, but is also a hydrophobic surface residue. Here I make a Hu I81A variant, mutating to the alanine seen in yeast cyt *c*. Our hypothesis was that this mutation would show a destabilization of the heme crevice loop region when monitoring the charge transfer band (695 nm), and more importantly observing an increase in peroxidase activity when monitoring for tetraguaiacol (470 nm) in our enzymatic assay. This signifies this mutation could have evolved to lock down that heme crevice loop in order to decrease peroxidase activity when intrinsic apoptosis pathways evolved in mammals. pH titration data showed a decrease in stability of the alkaline conformational transition in our I81A variant when compared to Hu WT. When looking at peroxidase activity we see a significant increase in $k_{cat}(s^{-1})$ values of I81A compared to Hu WT. The Hu I81A indeed shows what we would expect of a mutation which evolved to decrease peroxidase activity. Analysis of pH jump data in the Soret region of cyt*c* shows that there is an effect on lysine 73 or 79 bound alkaline ligands (unable to be determined) by a decrease in amplitude, however there is no effect on the lysine 72 bound alkaline ligand.

Acknowledgements

My work would not be possible without the close guidance of Dr. Bruce Bowler at the University of Montana. His kindness and compassion for teaching is surpassed by none. I feel that he defines what it means to do good science, and has fostered a curiosity in me that will hold strong for the remainder of my career. I also wish to acknowledge Dr. Charlotte Phillips at the University of Missouri, who taught me the scientific principles of research which I keep dear to this day.

I would also like to acknowledge my daughter Echo. Without her I would have never gone back to school in the first place. To my ex-wife Stephanie, thank you for all of the support you gave me so I could make it to where I am today. I wouldn't have made it through college without your motivation and model of hard work. For that I am truly grateful. To my girlfriend Bailey, I wish I could describe to you how much your support means to me.

Table of Contents

List of Figures

List of Tables

Chapter 1
Introduction

A. Proteins

Proteins are large polymers composed of amino acids which, apart from water, constitute the largest fraction of a cell (Levinthal 1968). Proteins are composed of amino acids of which there are 20 naturally occurring in our bodies. These can be grouped by their R-group/side chain, more specifically by those with positive or negative charges, those that are polar but do not contain a full charge, and those that are entirely hydrophobic along with other special cases.

Chains of amino acids are formed by the synthesis of peptide bonds via dehydration reactions (designated such because of each reaction's release of an H_2O molecule) which are shown in Figure 1.3. This is what forms the proteins primary sequence. It is from this repetitive synthesis that the protein code is made, leading to the formation of sequence groups which bias secondary structure characteristics, categorized as alpha helices, beta sheets, and random coil as shown in Figure 1.1. These are formed by the thermodynamic downhill folding of protein primary sequence. Christian Anfinsen's work, as summarized by Figure 1.2 shows that spontaneous folding occurs in proteins and more importantly, the only factor needed to determine the three-dimensional structure or gross fold within small globular proteins is the primary amino acid sequence. Anfinsen shows this by using the protein/enzyme ribonuclease which he denatures and breaks disulfide crosslinks with the use of Urea and mercaptoethanol, the reformation of the active state of ribonuclease indicates the driving force of the primary sequence. The experiment shown in Figure 1.2 was first described by Edgar Haber and Christian Anfinsen in 1962 (Haber and Anfinsen 1962) and later called the "Thermodynamic Hypothesis" by Anfinsen later in his career (Anfinsen 1973).

As diverse as they may be, neurodegenerative diseases have a common denominator of aberrant protein conformers and proteinaceous deposits (Winklhofer *et al* 2008). These diseases

include Alzheimer's disease, Parkinson's disease, Huntington's disease, amyotrophic lateral sclerosis, and prion diseases (Ross and Poirier 2004). Cytochrome *c*, apart from its component role in cellular electron transport, and intrinsic apoptosis, has also been identified to have negative secondary pathogenic effects such as that of psoriasis (Gabr and Al-Ghadir 2012) and hepatocellular carcinoma (Afify *et al* 2015). With cytochrome *c* such an active protein in biological function, the pressures, and specifically the residue by residue evolution which over time formed its role as an electron transporter and intrinsic apoptosis initiation factor remain of great interest to myself and others.

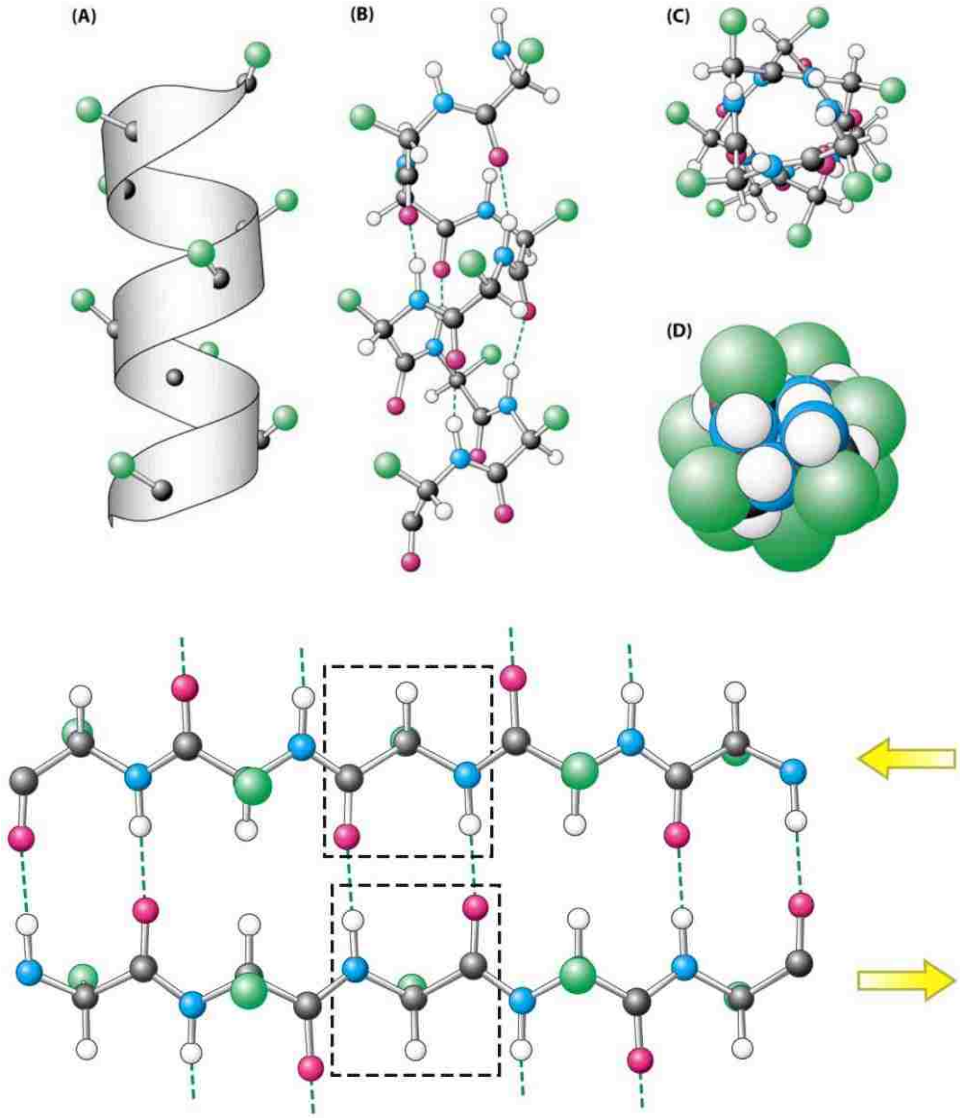

Figure 1.1 Common Secondary Structures of Proteins as taken from Figure 2.24 in Berg, Tymoczko and Stryer Biochemistry 6th edition. A-D show arrangements of an alpha helix and the lower half of the figure shows an anti-parallel β conformation as taken from Figure 2.31 in Berg, Tymoczko and Stryer Biochemistry, 7th Edition.

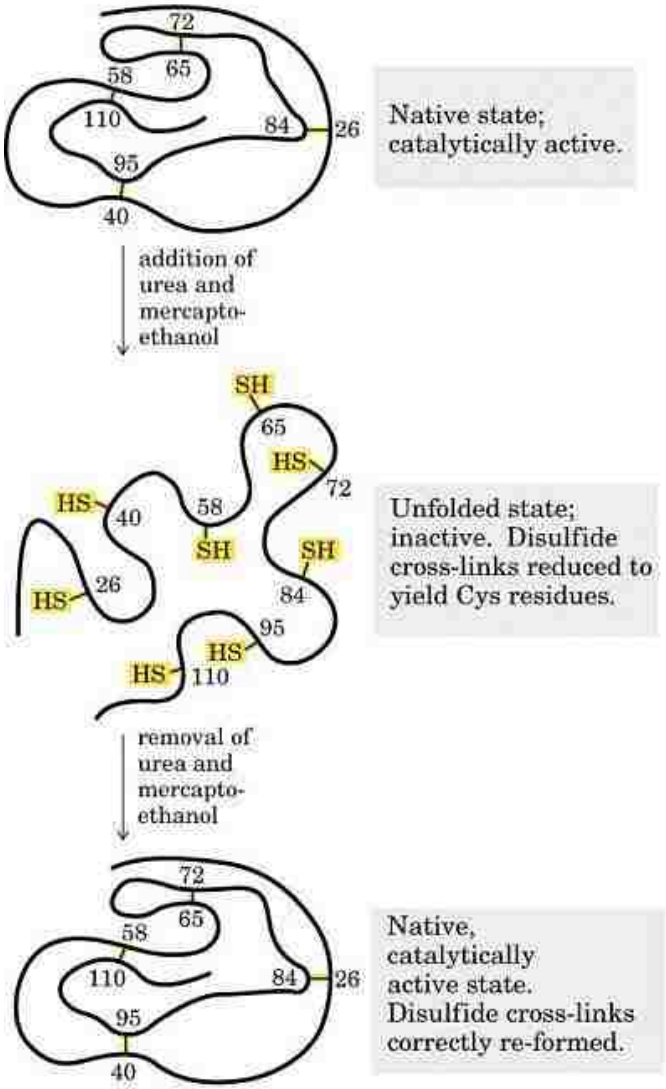

Figure 1.2 Renaturation of unfolded, denatured ribonuclease as taken from Figure 4-26 in Lehninger 5th Edition which describes the experimental procedure used by Christian Anfinsen in determining the responsibility of protein primary structure on its globular, folded form.

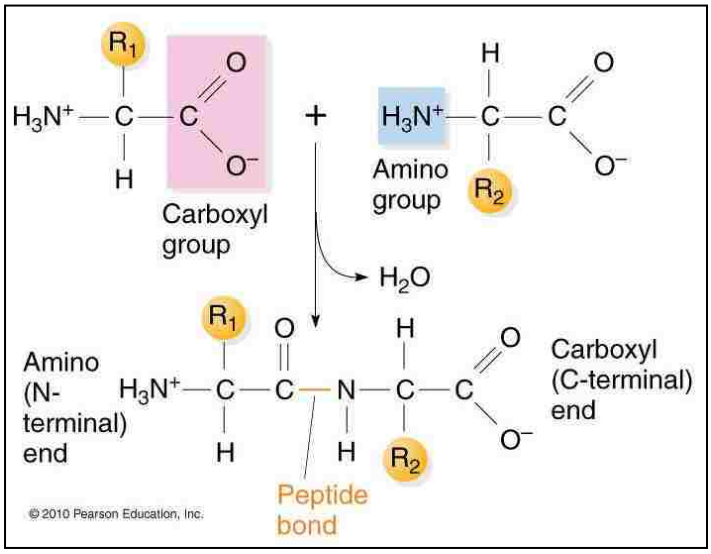

Figure 1.3 This figure is taken from 2010 PJ Russell, iGenetics 3rd edition. Here we see the dehydration reaction where the carboxyl group of amino acid R1 and the amino group of amino acid R2 combine to lose an H_2O and form a covalent peptide bond shown in the lower half of the figure.

B. Protein Folding Theory

Proteins are known widely as the building blocks of life. How proteins to fold into precise three dimensional structures has been an intense area of interest. A thought experiment by Cyrus Levinthal addresses the requirement for a guided folding process. His experiment works by showing the impossibility of conformational sampling of all ϕ and ψ angles (Figure 1.4) if all conformations and combinations are possible; this idea was coined Levinthal's Paradox (Levinthal 1968).

Such a guided process was later proposed by Christian Anfinsen in which the amino acid sequence itself was responsible for the structure and folding determination in small globular proteins; this was termed Anfinsen's Dogma (Anfinsen 1973) and has been the central motivator of mutagenesis directed at protein folding research in proteins such as cytochrome *c*.

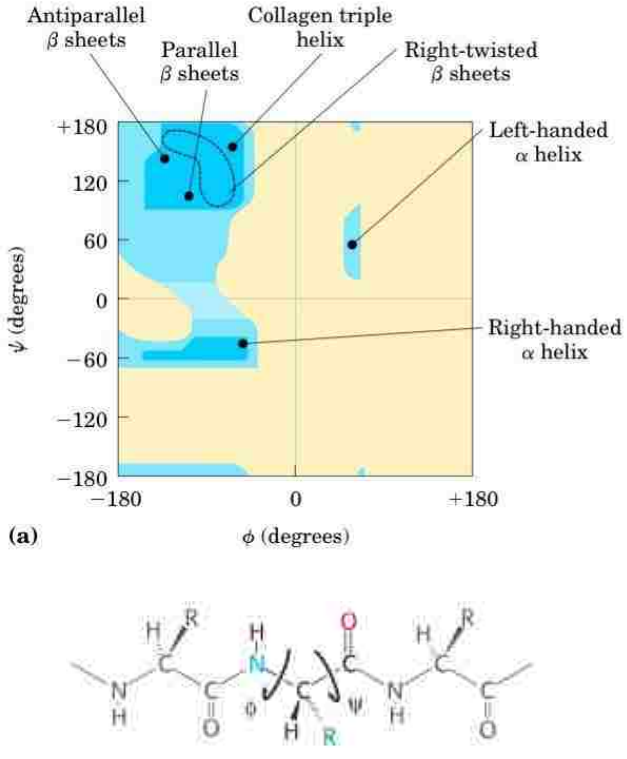

Figure 1.4 A Ramachandran plot as represented in figure 4-8(a) in Lehninger 5th Edition which describes the variety of secondary structures which an amino acid is theoretically able to attain based on φ and ψ angles, shown represented in figure 2.27 Stryer 6th Edition describing the rotation of bonds in a polypeptide

C. Cytochrome *c* Background

Cytochrome *c* is a small metalloprotein which, because of its covalently bound c-type heme is stable to a wide range of temperatures and pHs. This characteristic alone may be why it is so well studied in the scientific community. Its stability may allow in depth investigation into folding kinetics, dynamics, and heme chemistry among others, but its role as a model protein is not its greatest role. Cytochrome *c* is most well-known for its much larger roles as an electron transporter from cytochrome *c* reductase (Complex III) to cytochrome *c* oxidase (Complex IV) and as an apoptotic initiation factor in response to an initial increase in reactive oxygen species inside the mitochondria.

Different regions of cytochrome *c* may be responsible for different interactions with solvent, proteins, and macromolecules, among others. For example, residues 21-25 of cytochrome *c* are needed for destabilized structural change when initiating protein-protein interfaces with Complex III (Kokhan *et al* 2010). For interactions more relevant to the material which I will address in this thesis, I will save specific residues for the section discussing the heme crevice loop region of cytochrome *c* as this is where the mutations that I make take place.

D. Heme Crevice Loop

The heme-crevice loop, also known as the heme crevice loop foldon or omega loop-D, of cytochrome *c* consists of residues 70-85. Contained within the loop are three lysine residues at positions 72, 73, and 79. The heme crevice loop is the most highly conserved region of cytochrome *c* with 13 of the 16 amino acids being conserved between yeast and human cytochrome *c*. This is shown in Figure 1.5. Furthermore, the methionine residue at position 80, which is one of two axial bound residues (Histidine 18 being the other) that finds itself natively

bound to the heme iron, is also located within the heme crevice loop region, thus allowing the loop region to enclose one surface of the heme cofactor.

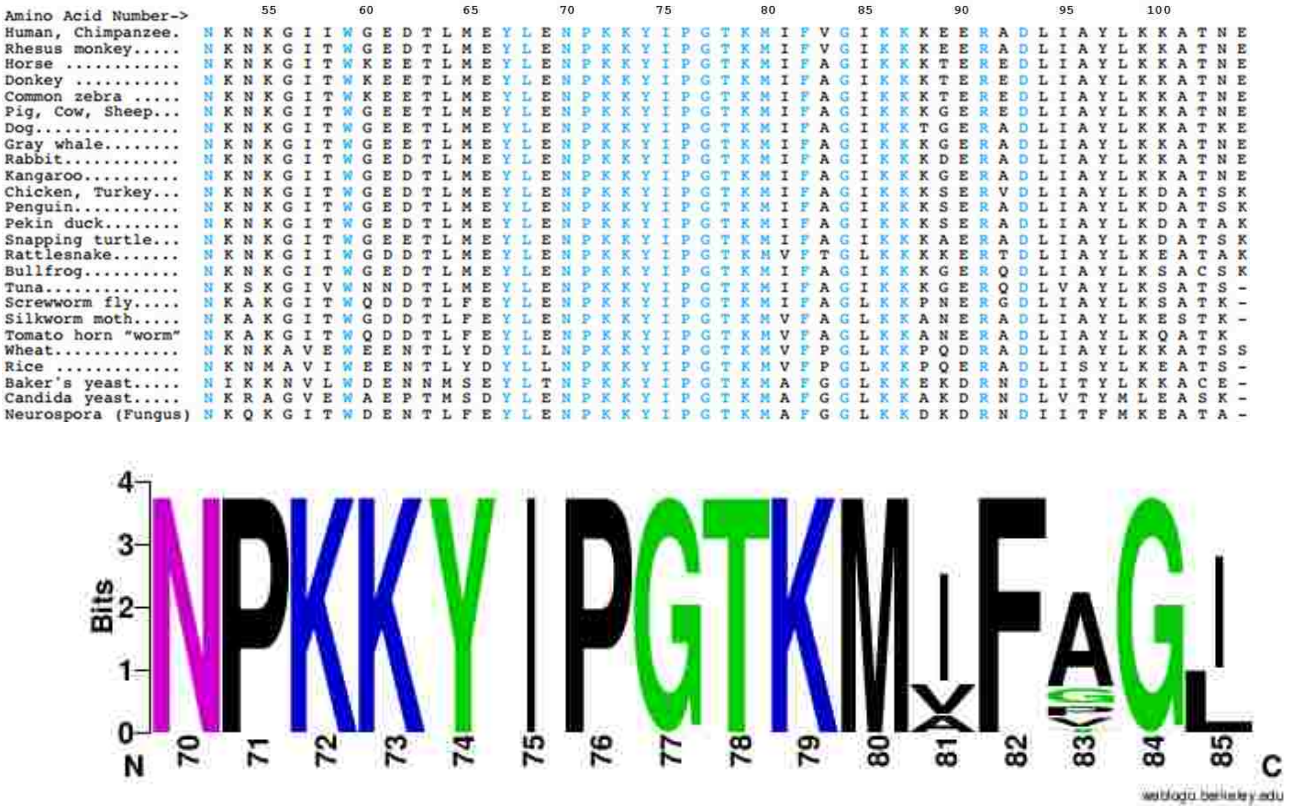

Figure 1.5 A sequence overlay of regions of cytochrome *c* taken from various organisms as taken from the Evolution and Nature of Science Institutes at the University of Indiana. The region in this figure shows residues 52 – 104. (Strahler 1987) Below this is a sequence logo of the heme crevice loop region of the sequences overlaid from the above sequence overlays containing residues 70 – 85. Colors represent amino acids chemistry with pink/purple being neutral amino acids, green being polar amino acids, blue being basic amino acids and black being hydrophobic amino acids. Height of each letter represents conservation.

E. Alkaline Conformational Transition

The alkaline conformational transition of cytochrome *c* is characterized by the alkaline induced loss of the natively bound methionine sulfur contact with the heme iron of cytochrome *c*. The increase in pH alkalinity allows residues, of which lysines 73 and 79 have been identified (Bandi *et al* 2007) to become deprotonated and displace methionine 80. Differences between native and alkaline conformers show heme crevice loop conformational changes shown in Figure1.6 (McClelland et al 2014). This leads us to hypothesize that the residue at positions 81

will provide significant deviation in the context of peroxidase activity, which translates to cellular apoptosis. I hypothesize that this effect is due to the residues K72 and I81 being important in controlling heme crevice stability. Changes in this stability alter the ability for M80-heme to block peroxidase activity, thus increasing overall peroxidase activity of Hu Cyt*c*.

In chapter 3, I will compare K72A to WT Hu Cyt*c*. I will discuss my findings specifically with regard to the role of K72 in altering Cyt*c* folding chemistry and the alkaline conformational transition, specifically affecting peroxidase activity. I will also discuss my findings on alkaline transition kinetics, where I will assign states based on pH jump data from WT and K72A Hu Cyt*c*.

In chapter 4, I will compare I81A to WT Hu Cyt*c*. I will discuss my findings within the context of what was seen with prior increase of heme crevice loop movement for A81 in yeast iso-1-cyt*c* (Figure 1.6) (McClelland et al 2014). I will discuss significant findings in global and local unfolding stability and peroxidase activity.

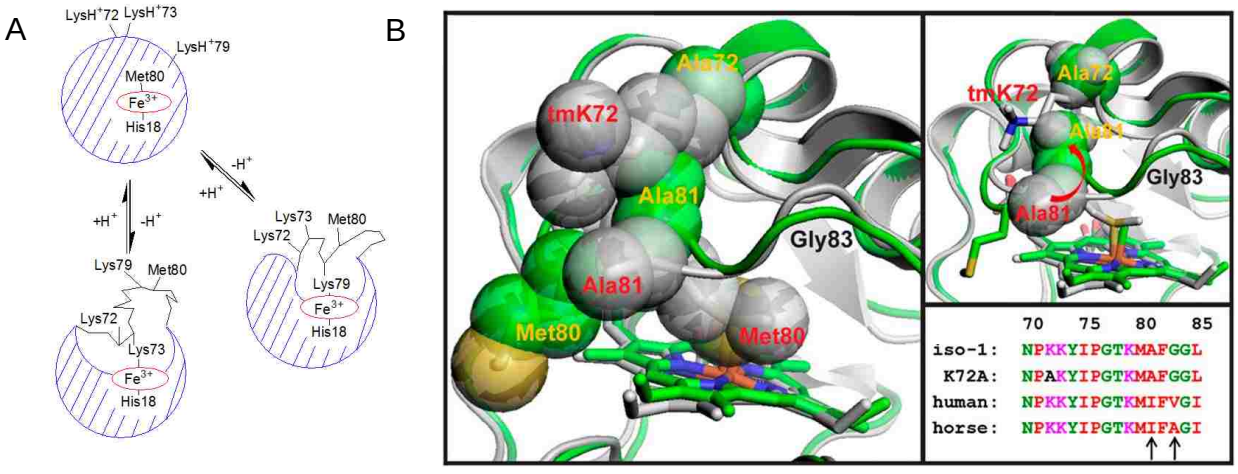

Figure 1.6 Heme crevice loop and the alkaline conformational transition of cyt *c*. A) shows the binding schematic of alternative lysine conformers at higher pH's that occur after deprotonation of nitrogen occur. B) shows the heme crevice loop movements that occur upon changes in native M80-heme iron binding, specifically changes in the position of A81.

Chapter 2
Methodology

A. Preparation of Cytochrome *c* and Variants

WT, I81A and K72A Hu Cyt*c* were prepared with site-directed mutagenesis using the pBTR(HumanCc) plasmid provided by the laboratory of Gary Pielak at the University of North Carolina (Olteanu *et al* 2003). pBTR(HumanCc) is derived from the pBTR1 plasmid (Rosell and Mauk 2002; Pollock *et al* 1998) through replacement of the yeast iso-1-Cyt*c* gene (*CYC1*) with a synthetic human cytochrome *c* gene (Olteanu *et al* 2003; Patel *et al* 2001). pBTR(HumanCc) like pBTR1 co-expresses the yeast heme lyase (*CYC3)* and uses it to covalently attach heme to the CSQCH heme recognition sequence of Hu Cyt*c*. Double-stranded pBTR(HumanCc) DNA was prepared using BL21-Gold(DE3) (Agilent Technologies) competent *Escherichia coli* cells and used as a template for site-directed mutagenesis with the Agilent Technologies QuikChange Lightning Site-Directed Mutagenesis Kit. For mutagenesis the following oligonucleotides were used:

K72A: d(GGAATACCTCGAGAACCCGGCGAAATACATCCCGGGCACG)

I81A: d(GGCACGAAAATGGCGTTCGGCGGCATCAAAAAAAAAGAAG)

These were used along with their reverse complements, K72A-r and I81A-r. The mutated DNA was transformed into TG-1 *E. coli* cells. Individual colonies were then grown in L-broth with Ampicillin (10 mL L-broth with 10 μL of 100 mg/mL Ampicillin) at 37 °C overnight. The DNA was extracted and purified with the Promega Wizard® *Plus* Miniprep DNA Purification System. The sequence was confirmed with an ABI 3130 Genetic Analyzer at the Genomics Core Facility at the University of Montana.

B. Expression, Extraction, Isolation and Purification of Hu Cyt*c*

WT , I81A and K72A Hu Cyt*c* were expressed from the pBTR(HumanCc) plasmid after transformation into Ultra BL21 (DE3) *E. coli* competent cells (EdgeBio, Gaithersburg, MD) using the manufacturers protocol. Sterile Fernbach flasks containing 1 L of 2xYT bacterial media were inoculated with 1 mL of cells from the L-ampicillin after all the cells on the plates were suspended in 3 mL of sterile L-broth. 1.5 mL of 100 mg/mL ampicillin and 100 μL of antifoam were also added to each Fernbach flask. The flasks were placed in an orbital shaker at 150 rpm and 37 °C for 30-40 hours. On average, a 1 L culture yielded 4.7 g of pelleted cells.

Protein extraction and purification were carried out as described, previously (Cherney *et al* 2013), (Redzic and Bowler 2005), (Wandschneider *et al* 2003), and (Goldes *et al* 2016). In brief, cell pellets were subjected to three freeze-thaw cycles, suspended in 50 mM Tris pH 8.0, 500 mM NaCl, and 1 mM EDTA and then passed through a French Pressure Cell to complete lysis. Four times the amount of lysis solution was used with 2 mM of PMSF where the lysis buffer amount was calculated using the template as shown:

(Mass of Cell Pellet)(4) = mL **Lysis Solution** needed

(mL of Lysis Solution from Step 2)(2mM) = (Amount of **PMSF** needed)(100mM)

mL Lysis Solution – mL of PMSF = mL of **Lysis Buffer** needed

A spatula tip full of DNAse and RNAase were also used for the lysis solution and the cell pellets were incubated at room temperature in the lysis solution with an orbital shaker for 1 hour. French Press was then performed with a Thermo IEC with a SLM-Aminco pressure cell for 10-20 cycles.

An ammonium sulfate cut was performed on the remaining cell lysates. 31.4 g of Ammonium sulfate was used for 100 mL of cell lysate. This leads to the following calculation:

(.314 g/mL)(XmL) = Grams of ammonium sulfate to add to lysates

The cleared lysate was adjusted to 50% ammonium sulfate, allowed to equilibrate overnight at 4 ^{o}C. After removing precipitated protein impurities, the supernatant was dialyzed against two changes of 12.5 mM sodium phosphate, pH 7.2, 1 mM Na_2EDTA, 2 mM β-mercaptoethanol (βME). The diasylate was stirred with 100 mL of CM-sepharose (GE Healthcare Life Science) to bind Hu Cyt*c* to the resin, and the resin was loaded into a glass column. After elution with a 200 mL linear gradient (0 – 0.8 M NaCl in 50 mM sodium phosphate pH 7.2, 1 mM Na_2EDTA, 2 mM βME), protein was exchanged into 50 mM sodium phosphate, pH 7 by centrifuge ultrafiltration, flash frozen in liquid N_2 and stored at -80 ^{o}C until used.

Prior to experiments, WT, I81A and K72A Hu Cyt*c* were purified by HPLC using a BioRad UNO S6 column, as previously described (Goldes *et al* 2016). An example elution curve is shown in Figure2.1. The Hu Cyt*c* was then oxidized with potassium ferricyanide, and simultaneously separated from the oxidant and exchanged into a buffer appropriate to the experiment using Sephadex G25 (GE Healthcare Life Sciences, superfine grade) chromatography as shown in Figure 2.2.

Purified proteins were characterized by MALDI-ToF mass spectrometry using a Bruker microflex mass spectrometer. For WT Hu Cyt*c*; 12,234.78 m/z (expected: 12,234.03 m/z), and for K72A Hu Cyt*c*, 12175.17 m/z (expected: 12,176.94 m/z).

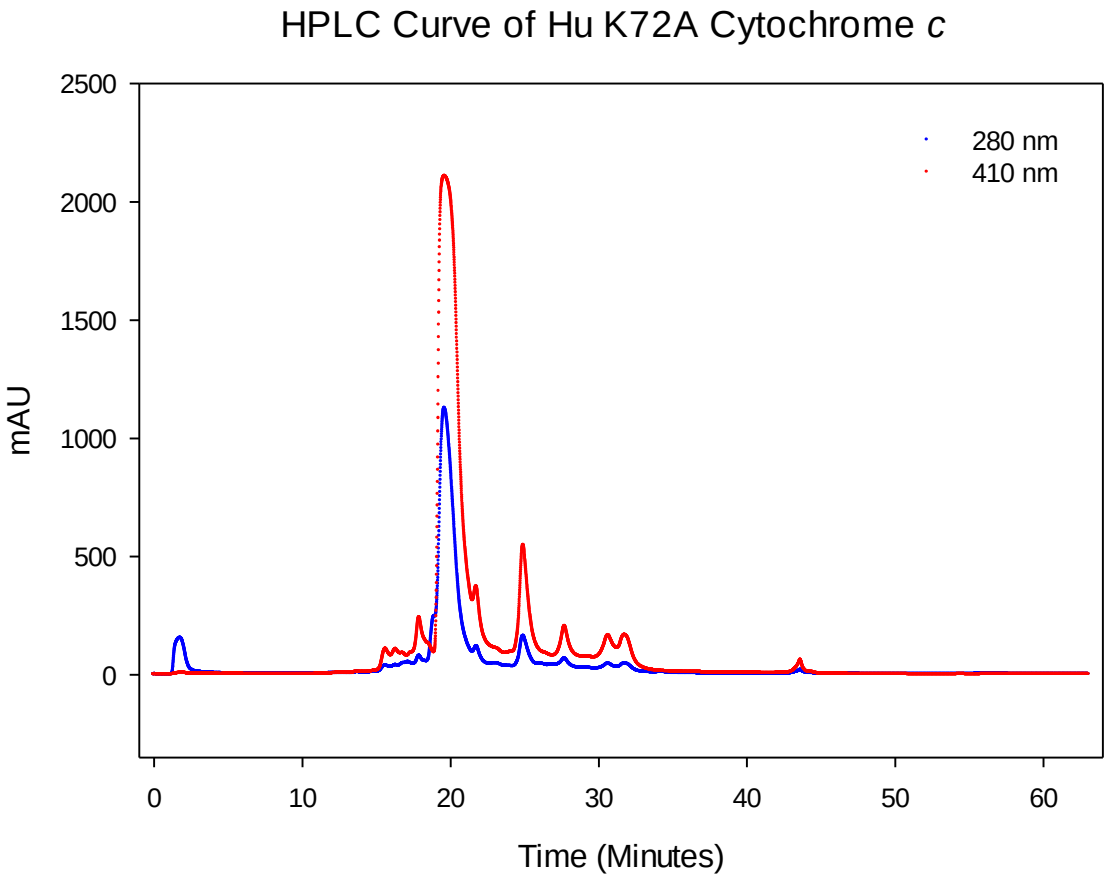

Figure 2.1 Example spectra for the HPLC separation of Hu K72A cytochrome *c*. Red spectra indicates absorbance at 410 nm and blue spectra indicates absorbance at 280 nm.

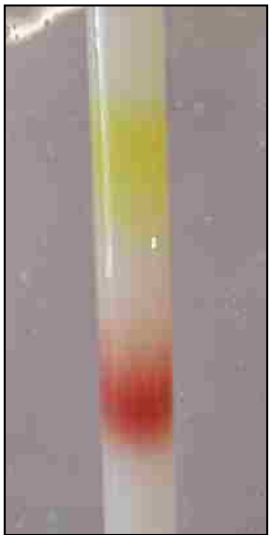

Figure 2.2 G-25 size exclusion chromatography of Hu Cyt*c*. Yellow band is ferricyanide. Red band is cytochrome *c*.

C. Crystallization and Structure Determination of Hu K72A Cyt*c*.

These experiments were carried out in collaboration with Haotian Lei and T.C. Mou. K72A Hu Cyt*c* was oxidized with $K_3[Fe(CN)_6]$, followed by separation from the oxidizing agent and exchange into 50 mM Tris pH 7 using Sephadex G-25 chromatography. It was then concentrated to ~16.5 mg/ml using centrifuge ultrafiltration (Amicon Ultra-4 10,000 MWCO). Screening for crystallization conditions was carried out using the JCSG core I, JCSG core II, JCSG core III, JCSG core IV, PEGS, PEGS II, Wizard classic 1&2, Wizard classic 3&4, Classic, Classic II, and Classic Lite commercial screening suites at 20 ^{o}C. The ratio of protein to reservoir solution in the drops in the 96 well sitting drop screening plates was 1:1. We obtained initial crystals from JCSG core I, well A2, which has a 0.1 M Bicine pH 8.5, 20%(w/v) PEG 6000 reservoir solution. Additional vapor diffusion crystallization experiments were set up in a 24-well VDX plate by expanding upon the pH and precipitant concentration of this initial condition. After 4 days to 2 weeks of equilibration at 20 ^{o}C, crystals were obtained from a drop containing 1 μL of protein and 1 μL of 25% PEG 6000, 0.1 M Tris pH 8, which diffracted to 1.8 Å at SSRL beamline 14-1. Further trials in the presence of sodium dodecyl sarcosine as an additive at 4.16 mM final concentration (60 mM stock) with a reservoir solution containing 30% PEG 3350 and 0.1 M sodium citrate, pH 6.4 and protein at 17.2 mg/mL (mixed 0.14:0.93:0.93) yielded crystals diffracting to 1.25 Å resolution in the P 2_1 space group. All crystals were cryoprotected with 20% glycerol and flash frozen in liquid N_2 for data collection.

The X-ray Diffraction dataset was collected under cryogenic conditions at 100 K at the SMB beamline 9-2 of the Stanford Synchrotron Radiation Lightsource (SSRL) using a Pilatus 6 M detector. Diffraction data were processed using HKL2000 (Otwinowski and Minor 1997). The initial electron density map was determined using phases obtained with the molecular

replacement method using Phaser, incorporated in the PHENIX software suite, (Adams *et al* 2010) and the coordinates of the wild-type human Cyt*c* structure (PDB ID: 3ZCF) as a search model. The initial model was built into a continuous electron density map and subsequently refined using PHENIX. The structure model was further refined to 1.25 Å resolution by multiple rounds of manual model rebuilding with COOT (Emsley *et al* 2010) and restrained refinement with PHENIX using 5 % of reflections for calculation of R_{free} (Table 1). Data collection and refinement statistics of the final model are summarized in Table 1. The coordinates and structure factors for K72A Hu Cyt*c* mutant have been deposited in the Protein Data Bank (PDB ID: 5TY3).

Table 2.1. X-ray crystallography and data collection and refinement statistics.

PDB ID	5TY3
Beamline	SSRL SMB 9-2
Wavelength (Å)	1.07
Resolution range (Å)	25.00-1.25 (1.29-1.25)*
Space group	P 2_1
Unit cell dimensions	
a, b, c (Å)	56.8, 37.9, 60.3
α, β, γ (◦)	90, 116.8, 90
Total reflections	1539904
Unique reflections	62478 (5985)*
Redundancy	6.5 (5.3)*
Completeness (%)	97.8 (93.6)*
Mean I/σ(I)	24.5 (6.1)*
Wilson B-factor	10.85
R_{sym} †	0.07 (0.27)*
Refinement	
R_{work} §	0.147 (0.194)*
R_{free} §	0.166 (0.201)*
Number of total atoms	2204
protein	1660
ligands	96
solvent	448
Total protein residues	210
RMS (bonds, Å)	0.017
RMS (angles, ◦)	1.38
Ramachandran favored (%)††	98
Rotamer outliers (%)††	0.2
Average B-factor	17.69
macromolecules	14.89
ligands	11.44
solvent	29.40

*Data for highest resolution shell are given in brackets. †$R_{sym} = \sum_{hkl} \sum_i | I_i (hkl) - \langle I (hkl) \rangle | / \sum_{hkl} \sum_i I_i (hkl)$ where $I_i (hkl)$ is the *i*th observation of the intensity of the reflection *hkl*. §$R_{work} = \sum_{hkl} || F_{obs}| - |F_{calc}|| / \sum_{hkl} |F_{obs}|$, where F_{obs} and F_{calc} are the observed and calculated structure-factor amplitudes for each reflection *hkl*. R_{free} was calculated with 5% of the diffraction data that were selected randomly and excluded from refinement. ††Calculated using MolProbity.[26]

D. Global Unfolding Thermodynamics using Guanidine Hydrochloride and Circular Dichroism Spectroscopy

Global unfolding thermodynamics of WT, I81A, and K72A Hu Cyt*c* were determined by guanidine hydrochloride (GdnHCl) denaturation monitored by circular dichroism (CD) spectroscopy. Protein was oxidized with potassium ferricyanide and separated from oxidant by G-25 size exclusion chromatography in CD buffer (20 mM Tris, pH 7.5, 40 mM NaCl). Concentration of GdnHCl was determined using a Fisher Scientific refractometer. Calculation of GdnHCl concentration was done using the empirical equation of Nozaki for the change in refractive index relative to the background buffer (Nozaki 1972).

GdnHCl unfolding titrations were carried out with an Applied Photophysics Chirascan CD Spectrophotometer coupled to a Hamilton Microlab 500 Titrator. The change in ellipticity was monitored at 222 nm using 250 nm as background, $\theta_{222corr}$ (θ_{222nm} - θ_{250nm}). The protein concentration was 4 μM. $\theta_{222corr}$ versus GdnHCl concentration denaturation curves were fit to equation 2, which assumes two state unfolding and a linear dependence of the free energy of unfolding, ΔG_u, on GdnHCl concentration (Pace *et al* 1989; Schellman 1978). Native and denatured state baselines were also varied linearly with GdnHCl concentration. In eq 2.1, θ_N and m_N are the slope and the intercept of the native state baseline, θ_D and m_D are the slope and the intercept of the denatured state baseline, m is slope of ΔG_u with respect to GdnHCl concentration and $\Delta G_u^{o'}(H_2O)$ is the free energy of unfolding extrapolated to 0 M GdnHCl.

Equation 2.1 Protein Denaturation by Guanidine HCl

$$\theta_{222corr} = \frac{\left[(\theta_{\mathrm{N}} + m_{\mathrm{N}}[\mathrm{GdnHCl}]) + (\theta_{\mathrm{D}} + m_{\mathrm{D}}[\mathrm{GdnHCl}]) \cdot \exp\left\{\frac{m[\mathrm{GdnHCl}] - \Delta G_{\mathrm{u}}^{\circ\prime}(\mathrm{H_2O})}{RT}\right\}\right]}{1 + \exp\left[\frac{m[\mathrm{GdnHCl}] - \Delta G_{\mathrm{u}}^{\circ\prime}(\mathrm{H_2O})}{RT}\right]}$$

E. pH-Titrations using Ultraviolet-Visible Spectroscopy

The alkaline conformational transition of WT, I81A, and K72A Hu Cyt*c* was monitored with a Beckman DU800 spectrophotometer with absorbance at 695 nm, A_{695}, a weak absorbance band which reports on the Met80-heme ligation of the native state (Moore and Pettigrew 1990). The absorbance data were corrected for baseline drift using absorbance at 750 nm, A_{750}, as baseline ($A_{695corr} = A_{695} - A_{750}$). Titrations were monitored at room temperature (22 ± 3 °C) with 200 μM protein in 100 mM NaCl. Titrations were carried out by adding equal amounts of an appropriate concentration of NaOH along with a 2x protein stock (400 μM protein in 200 mM NaCl) to keep protein concentration constant throughout the experiment (Kristinsson and Bowler 2005; Nelson and Bowler 2000). Plots of $A_{695corr}$ versus pH were used to determine the apparent pK_a (pK_{app}) by fitting the data to Equation 2.2, a modified form of the Henderson-Hasselbalch equation that evaluates the number of protons, *n*, linked to the alkaline conformational transition. In Equation 2.2, A_N and A_{alk} are the corrected absorbance at 695 nm of the native and alkaline conformers, respectively.

Equation 2.2 Modified Henderson Hasselbalch Equation for determination of pK_{app}

$$A_{695\mathrm{corr}} = \frac{A_{\mathrm{N}} + A_{\mathrm{Alk}} \times 10^{n[\mathrm{p}K_{\mathrm{app}} - \mathrm{pH}]}}{1 + 10^{n[\mathrm{p}K_{\mathrm{app}} - \mathrm{pH}]}}$$

F. pH Jump Stopped-flow Kinetic Measurements.

Kinetics of the alkaline conformation transition were monitored via pH jump stopped-flow experiments carried out with an Applied Photophysics SX20 stopped-flow apparatus at 25 °C. The conformational transition was monitored at 406 nm in the heme Soret region. Oxidized protein (Fe(III)-heme) was separated from ferricyanide using a G25 column equilibrated to and run with 0.1 M NaCl. The solution was adjusted to 20 μM protein concentration and pH 6 for upward pH jumps and to near pH 10 for downward pH jumps. 1:1 mixing with 0.1 M NaCl containing 20 mM buffer yields a final protein concentration of 10 μM in 10 mM buffer, 0.1 M NaCl. Buffers used for pH jump stopped-flow were: MES, pH 5.5 – 6.5; NaH_2PO_4, pH 6.75 – 7.5; Tris, pH 7.75 – 8.75; Boric Acid, pH 9.0 – 10.0; CAPS, pH 10.25 – 11:0. Samples were taken from the Stopped-Flow waste line and pH was measured directly after mixing experiments at each pH. Data were fit to one – four exponential equations as appropriate:

Equation 2.3 Single Exponential Equation Fit

$$f = y_o + a_1\,(1 - \exp(-k_1 * x))$$

Equation 2.4 Double Exponential Equation Fit

$$f = y_o + a_1\,(1 - \exp(-k_1 * x)) + a_2(1 - \exp(-k_2 * x))$$

Equation 2.5 Triple Exponential Equation Fit

$$f = y_o + a_1\,(1 - \exp(-k_1 * x)) + a_2(1 - \exp(-k_2 * x)) + a_3(1 - \exp(-k_3 * x))$$

Equation 2.6 Quadruple Exponential Equation Fit

$$f = y_o + a_1\,(1 - \exp(-k_1 * x)) + a_2(1 - \exp(-k_2 * x)) + a_3(1 - \exp(-k_3 * x)) + a_4(1 - \exp(-k_4 *))$$

G. Peroxidase Activity Measurements.

Peroxidase activity was measured using the colorimetric reagent, guaiacol, using previously reported conditions and procedures (McClelland 2014; Wang *et al* 2011). The reaction was monitored using an Applied Photophysics SX20 stopped-flow apparatus at 25 °C. The formation of tetraguaiacol from guaiacol and H_2O_2 in the presence of Cyt*c* is monitored at 470 nm. 4x Cyt*c* (4 μM) in 50 mM buffer was mixed with 4x guaiacol in 50 mM buffer to produce a 2x Cyt*c* 2x guaiacol stock in 50 mM buffer. This solution was mixed 1:1 with 2x H_2O_2 (100 mM) in 50 mM buffer yielding a final solution containing 1 μM Cyt*c*, 50 mM H_2O_2 and guaiacol at the desired concentration in 50 mM buffer as shown in Scheme 2.1. Concentration was determined using the extinction coefficients of H_2O_2 (ε_{240} = 41.5 M^{-1} cm^{-1}, the average of published values (Nelson and Kiesow 1972; Noble and Gibson 1970) and guaiacol (ε_{274} = 2,150 M^{-1} cm^{-1}; Goldschmid 1953). Buffers used for peroxidase experiments were the same as those used in pH-Jump experiments. Concentrations of Guaiacol used for experimentation are 0, 2, 4, 6, 8, 10, 15, 20, 25, 30, 40, 50, 60, 80, 100, 150 and 200 μM concentrations.

Data were fit using Sigma Plot (Systat Software, Inc.). The segment of the A_{470} versus time data with the greatest slope following the initial lag phase was used to obtain initial velocity, *v*, at each guaiacol concentration. The data were fit to a linear equation and the slope from five repeats was averaged. The slope (dA_{470}/dt) was divided by the extinction coefficient of tetraguaiacol at 470 nm (ε_{470} = 26.6 $mM^{-1}cm^{-1}$; Diederix *et al* 2001) and multiplied by 4 to produce the initial rate of guaiacol consumption, *v*. The initial rate, *v*, was divided by cytochrome *c* concentration, plotted against guaiacol concentration and fit with Equation 2.7 to obtain K_m and k_{cat} values.

Equation 2.7 Used for the obtainment of K_m and k_{cat} values

$$\frac{v}{[\mathrm{Cyt}c]} = \frac{k_{cat} \cdot x}{K_m + x}$$

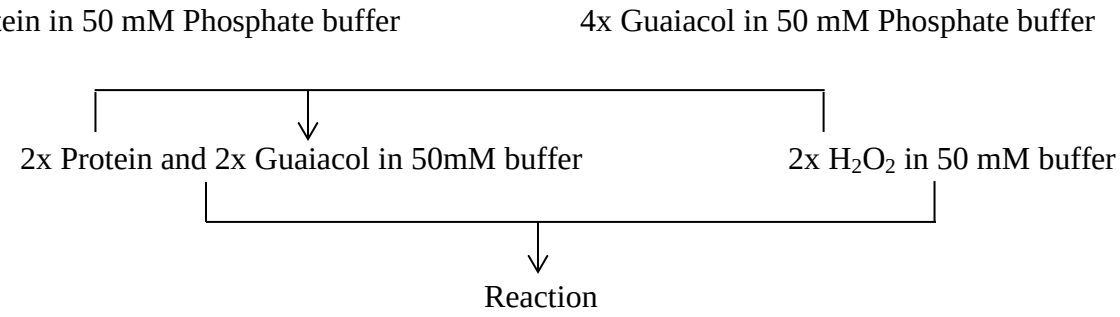

Scheme 2.1 A schematic representation of the dilutions that take place first in the premixing step and in the mixing cell of the stopped flow during peroxidase experiments.

Chapter 3
Significance of Lysine Residue 72 in Human Cytochrome *c*

A. Introduction of Hu K72A Hu Cyt*c*

The role of K72 in Hu Cyt*c* has been poorly defined in the literature. K72 has opposed functions and contributions in other Cyt*c* types. For example, in Yeast Cyt*c* mutation of the trimethylated lysine 72, tmK72, is known to regulate the opening of the heme-crevice loop as well as peroxidase activity (Cherney *et al* 2013; McClelland *et al* 2014). In Equine Cyt*c* similar investigation into K72 shows little contribution to the alkaline conformational transition (Maity *et al* 2006). This inconsistency in heme crevice loop dynamics and peroxidase activity leads us to investigate the role of K72 in Hu Cyt*c*.

B. Structure of K72A Hu Cyt*c*

Crystals of K72A Hu Cyt*c* were prepared in the absence and presence of sodium dodecyl sarcosine as an additive. In both cases, the K72A Hu Cyt*c* crystallized in the P 2_1 space group. The crystal obtained in the presence of the additive diffracted to a resolution of 1.25 Å (Table 2.1). A high quality structural model with R_{work}/R_{free} of 0.15/0.17 (Table 2.1) was obtained. Figure 3.1 shows an overlay of the K72A Hu Cyt*c* structure with that of WT Hu Cyt*c*. The structures are very similar. An all atom alignment of the K72A Hu Cyt*c* structure with the WT Hu Cyt*c* crystal structure (PDB ID: 3ZCF; Rajagopal *et al* 2013); PyMol align function using chain A of each structure) yields an RMSD of 0.18 Å. The methyl side chain of Ala72 of K72A Hu Cyt*c* is in the same position as the β-carbon of Lys72 of WT Hu Cyt*c* (Figure 3.1).

Lys72 of horse Cyt*c* (Bushnell *et al* 1990) and trimethyllysine72 (tmK72) of yeast iso-1-Cyt*c* (Berghuis and Brayer 1992) both lie across Ω-loop D making contacts with residues 80 to 82 on the far side of the loop. In the case of horse Cyt*c*, Lys72 makes three hydrogen bonds to backbone atoms of Met80 and Phe82 (Figure 3.2). In our previous work on a K72A variant of iso-1-Cyt*c*, (McClelland *et al* 2014) we proposed that removal of this cross loop interaction by

replacement of tmK72 with alanine labilized Ω-loop D permitting enhanced peroxidase activity. Thus, it seemed likely that a similar phenomenon might be operative for Hu Cyt*c*. However, in the structure of WT Hu Cyt*c*, Lys72 does not make direct contacts with the backbone atoms of Met80 and Phe82 as seen for horse Cyt*c*. In chain A of the WT Hu Cyt*c* crystal structure, Lys72 makes water-mediated contacts with the backbone atoms of Thr78, Met80 and Phe82 (Figure 3.2B). In our K72A Hu Cyt*c* crystal structure, the position of the ε-NH_2 group of Lys72 in chain A of the WT structure is occupied by a water molecule (Figure 3.2C). In the WT Hu Cyt*c* crystal structure, Lys72 makes water-mediated contacts with the backbone atoms of Thr78, Met80 and Phe82 (Figure 3.2B). In our K72A Hu Cyt*c* crystal structure, the position of the ε-NH_2 group of Lys72 in chain A of the WT structure is occupied by a water molecule (Figure 3.2C). However, in the other three molecules in the asymmetric unit of the WT Hu Cyt*c* crystal structure, the hydrogen bond network around Lys72 does not lead to cross loop contacts (Figure 3.3). Instead, the water mediated cross loop interactions in these molecules of WT Hu Cyt*c* are similar in to those in the two molecules in the asymmetric units of our K72A Hu Cyt*c* structure (Figures 3.2C and 3.4). In particular, irrespective of the presence of lysine at position 72, there is always a hydrogen bond between the carbonyl of Leu68 and the amide NH of Ile 85 at the neck of Ω-loop D (Figures 3.2, 3.3, and 3.4). Similarly, there is always a water-mediated hydrogen bond between the amide NH of residue 72 and the carbonyl of Phe82, which is often further supported by a water-mediated hydrogen bond to the side chain of Asn70 (Figures 3.2, 3.3, and 3.4). In many cases the water-mediated hydrogen bond network extends the entire length of Ω-loop D.

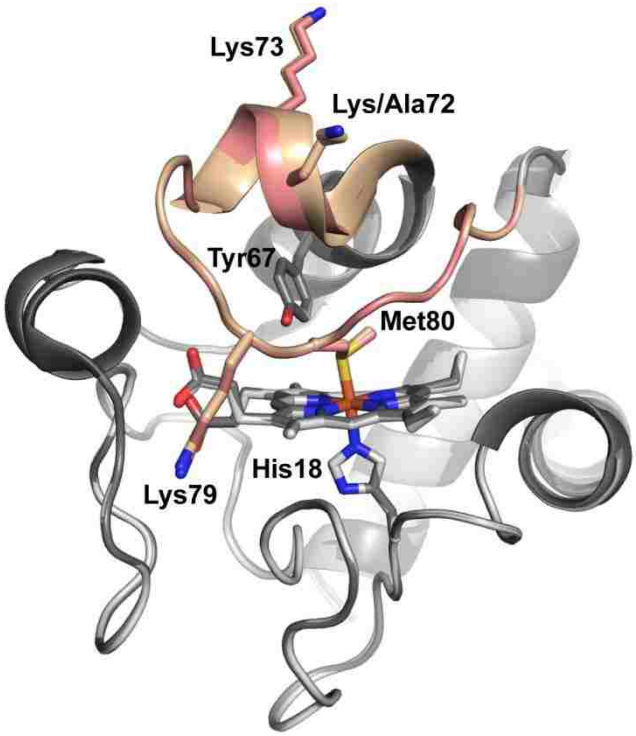

Figure 3.1 Overlay of the structures of K72A Hu Cyt*c* (PDB ID: 5TY3) and WT Hu Cyt*c* (PDB ID: 3ZCF). The K72A variant is shown in light gray and WT Hu Cyt*c* is shown in dark gray. The heme-crevice loop (Ω-loop D, residues 70-85) is highlighted in salmon for the K72A variant and tan for WT Hu Cyt*c*. The heme and its environment, Met80, His18, and Tyr 67, are shown as stick models. The three lysine residues in Ω-loop D (Lys/Ala72, Lys73 and Lys79) are also shown as stick models.

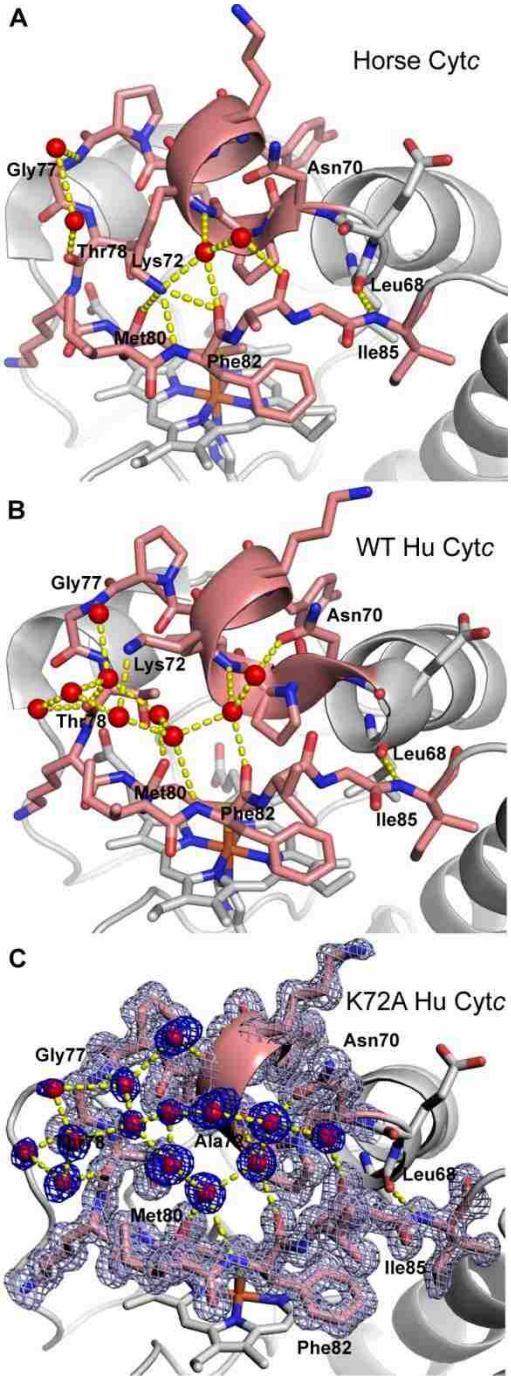

Figure 3.2 Hydrogen bond network across Ω-loop D. (A) Horse Cyt*c* (PDB ID: 1HRC) (B) WT Hu Cyt*c* (PDB ID: 3ZCF, chain A) and (C) K72A Hu Cyt*c* (PDB ID: 5TY3, chain A). Ω-loop D is colored salmon. Residues in the H-bond network are labeled. Waters are shown as red spheres and hydrogen bonds as yellow dashed lines. In part (C) the $2mF_o$-F_c electron density map for Ω-loop D (light blue) and for the waters (dark blue) is contoured at 1.2σ.

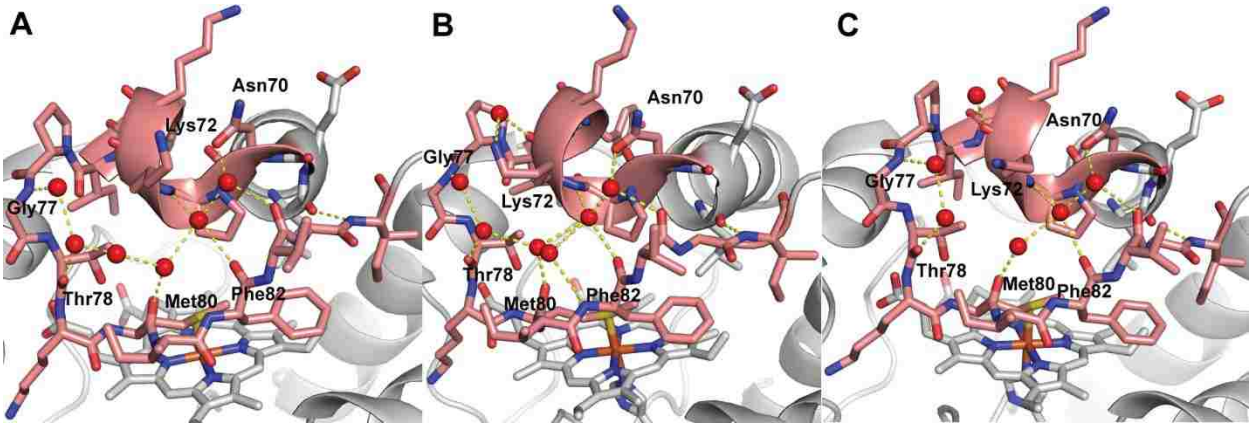

Figure 3.3 Hydrogen bond network for (A) chain B, (B) chain C, and (D) chain D of the asymmetric unit of Hu Cyt*c* (PDB code: 3ZCF). Ω-loop D is shown in salmon. Side chains in Ω-loop D are shown with stick models colored by element (carbon is salmon). Hydrogen bonds are shown as yellow dashed lines and waters are shown as red spheres. Residues involved in the hydrogen bond network are labelled.

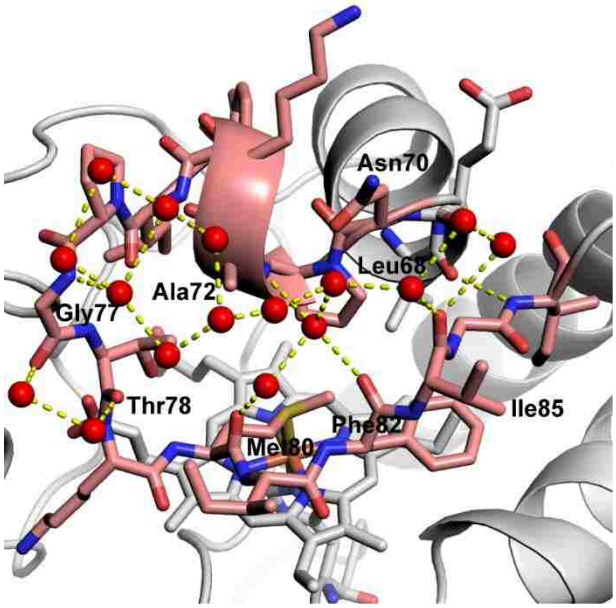

Figure 3.4 Hydrogen bond network for chain B of the 1.25 Å structure of K72A Hu Cyt*c* (PDB code: 5TY3). Ω-loop D is shown in salmon. Side chains in Ω-loop D are shown with stick models colored by element (carbon is salmon). Hydrogen bonds are shown as yellow dashed lines and waters are shown as red spheres. Residues involved in the hydrogen bond network are labelled.

C. Global Unfolding Thermodynamics of K72A Hu Cyt*c*

Global unfolding thermodynamics of Hu WT and Hu K72A were investigated using the denaturant guanidine hydrochloride, Gdn HCl, and denaturation curves were created via Circular Dichroism, CD at 25 °C and pH 7.5. As shown in Figure 3.5, little variation in these curves is seen comparing the Hu WT to Hu K72A when comparing corrected ellipticity ($\theta_{222corr} = \theta_{222nm} - \theta_{250nm}$) for monitoring our primary alpha helical protein. A small shift is however seen as indicated in Table 2.1 by stabilization in unfolding midpoints from 2.55 ± 0.01 M to 2.75 ± 0.03 M. This result is typical for single variant cytochrome *c* proteins and indicates that protein stability on a global level is not strongly altered due to the K72A mutation.

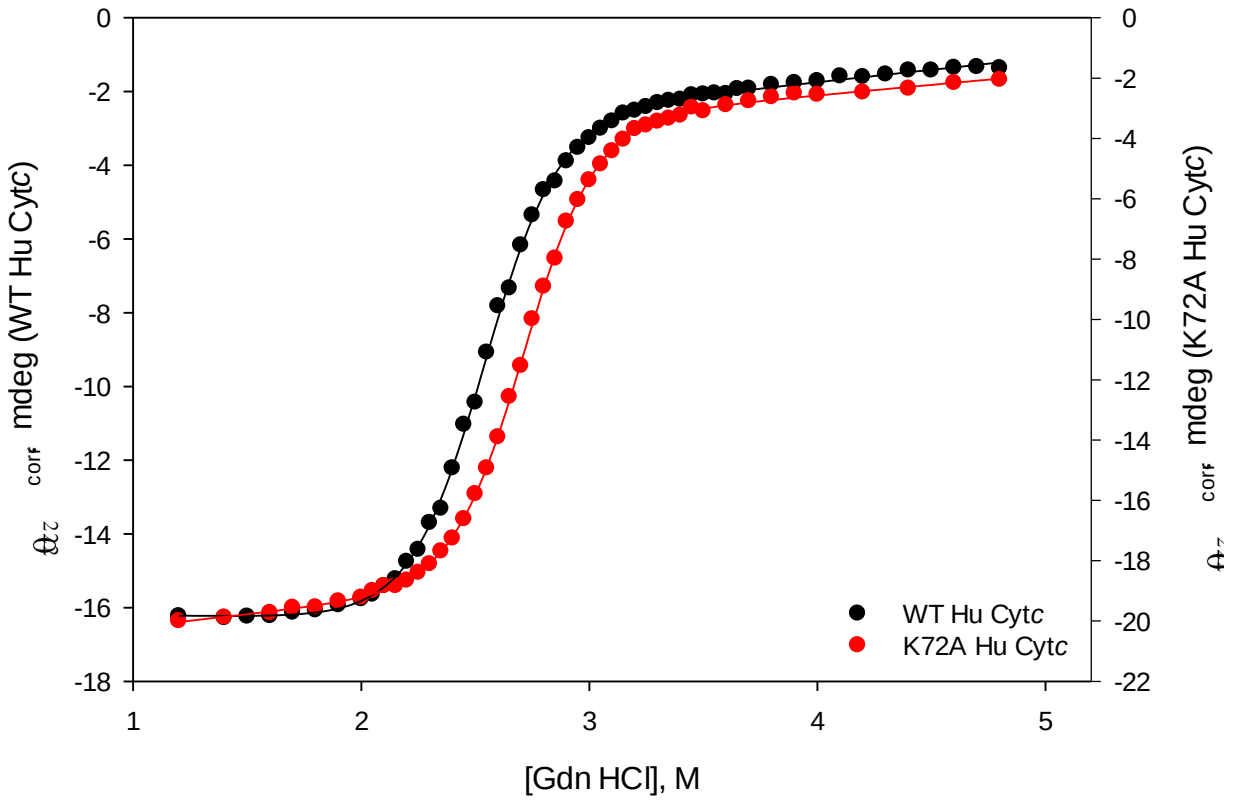

Figure 3.5: GdnHCl denaturation curves of WT Hu Cyt*c* (black) and K72A Hu Cyt*c* (red) shown as plots of corrected ellipticity, $\theta_{222corr} = \theta_{(222\ nm\ -250\ nm)}$, versus GdnHCl concentration. Curves shown as fits to Equation 2.1 with parameters obtained being listed in Table 3.1. Experiments were performed at 25 °C in CD Buffer (20 mM Tris, 40 mM NaCl, pH 7.5) at 4 μM protein concentration. Previously reported data for WT Hu Cyt*c* (Goldes *et al* 2016) are refit here.

Table 3.1. Thermodynamic parameters for global unfolding of WT and K72A Hu Cyt*c*.

Variant	*m* (kcal mol^{-1} M^{-1})	$\Delta G_u^{o'}(H_2O)$ (kcal mol^{-1})	C_m(M)
WT	3.71±0.05	9.46±0.11	2.55±0.01
K72A	3.64±0.15	10.01±0.30	2.75±0.03

The Hu WT data had previously been fit by our lab with a constant native state baseline model (Goldes *et al* 2016) but was fit here with a variable native state baseline model (equation 2.1) to be more directly comparable to the data of Hu K72A. Firstly, the denaturant *m* value is unchanged within error between the two as shown in Table 3.1. The $\Delta G_u^{o'}(H_2O)$ differs by roughly 0.5 kcal mol^{-1} with a small stabilization in the K72A variant which is also seen as a slight increase in melting midpoint concentration, C_m.

D. Alkaline Conformational Transition Thermodynamics of K72A Hu Cyt*c*

The alkaline conformational transitions of Hu WT and Hu K72A cytochrome *c* were monitored at the charge transfer band (695 nm) for the loss the Met80-heme iron ligation as an increase in pH occurs. A loss in absorbance occurs in this region due to the newly deprotonated lysine residues in the heme crevice loop region that bind at higher pH displacing the natively bound methionine. Figure 3.6 shows the pH titration comparison between Hu WT and Hu K72A. A clear stabilization is seen in the Hu K72A variant. Table 3.2 shows a shift in $pK_{a(app)}$ from 9.54±0.03 in WT to 10.0±0.1 in K72A using fits to the curves from equation 2.2. The number of protons linked to the alkaline transition is near 1 for both WT Hu Cyt*c* (n = 1.03 ± 0.02) (Goldes *et al* 2016) and K72A Hu Cyt*c* (n = 0.98 ± 0.06).

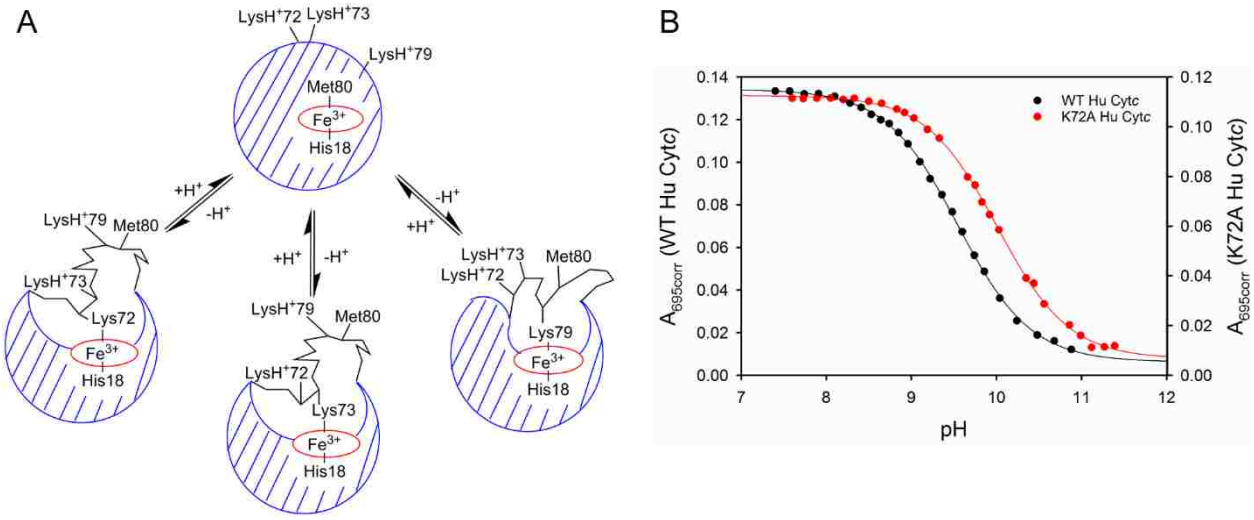

Figure 3.6: (A) Schematic representation of the alkaline conformational transition for Hu Cyt*c* showing all three possible alkaline conformers with lysines from Ω-loop D as alkaline state ligands. (B) Plots of $A_{695corr}$ versus pH for the alkaline transition for WT (black) and K72A (red) Hu Cyt*c*. Data were collected at room temperature (22 ± 3 °C) in 0.1 M NaCl solution with a protein concentration of 100 μM. Solid lines are fits to eq 2.2 in Chapter 2.

Table 3.2 Local Unfolding Thermodynamics of Hu WT and Hu K72A Cytochrome *c*. Data obtained by fits to the modified Henderson-Hasselbalch equation (Equation 2.2)

Variant	$pK_{a(app)}$	n
Hu WT	9.54±0.03	1.03±0.02
Hu K72A	10.00±0.13	0.98±0.06

Data shown in Table 3.2 show the $pK_{a(app)}$ of Hu WT and Hu K72A. $pK_{a(app)}$ values as determined by curves fit to equation 2.2 show the stabilization of Hu K72A native state to a higher pH regime compared to that of Hu WT. One interpretation is laid out in Figure 3.7. This model shows K72 in Hu Cyt*c* acting as heme bound ligand at higher pHs. This hypothesis is consistent with the observation that M80-heme is stabilized with K72 removal, as less possible heme binding ligands are present. However, kinetic data indicate another explanation might be the loss of proline isomerization in the primary phase when lysine is mutated to an alanine at position 72 (see next section).

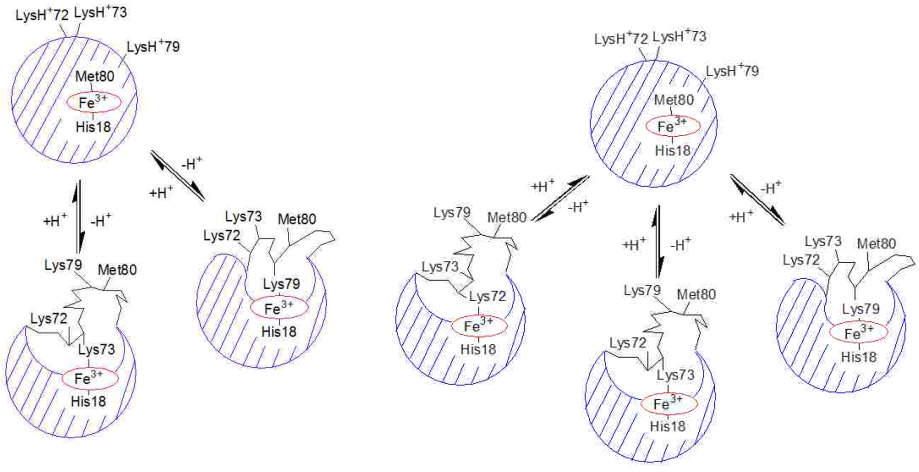

Figure 3.7 Our proposed schematic with the addition of K72 as a binding ligand in the alkaline conformational transition of Hu Cytochrome *c*. The left shows the initial scheme with the top conformer being the natively bound Met80-heme. As pH increases the lysines deprotonate and bind to the heme iron as alternative conformers shown in the lower half of the figure. The right shows the addition of the lysine at position 72 as an additional binding ligand as originally hypothesized by experimentation.

E. Alkaline Conformational Transition Kinetics

The local unfolding thermodynamics for the alkaline conformational transition of WT and K72A Hu Cyt*c* were determined by pH titration, monitored at 695 nm to observe the loss of Met80-heme iron ligation (Moore and Pettigrew 1990), when a lysine from Ω-loop D binds to the heme. A schematic representation of the human alkaline conformational transition is shown in Figure 3.6A. Lysines 72, 73 and 79 could all potentially bind to the heme. However, while all three lysines contribute to the alkaline conformer of yeast iso-1-Cyt*c* expressed from *E. coli*, (Pollock *et al* 1998), NMR studies suggest only two distinguishable alkaline conformers exist for horse Cyt*c* (Hong and Dixon 1986). Mutational analysis indicates that lysines 73 and 79 contribute to the alkaline transition of horse Cyt*c*, but that Lys72 does not (Cherney *et al* 2013).

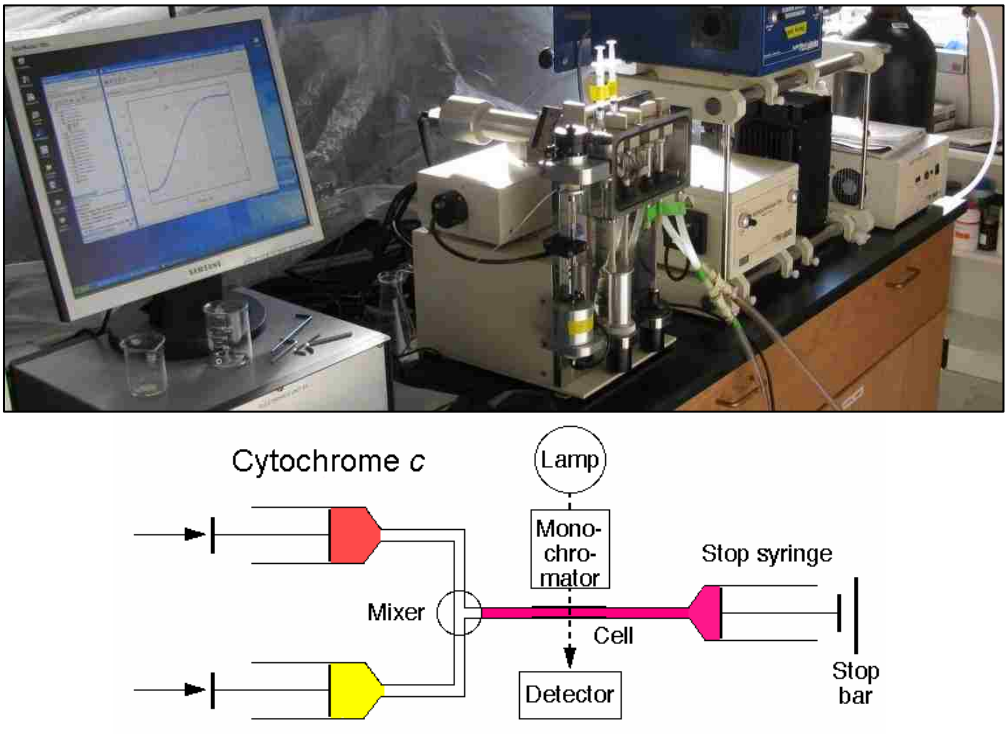

Figure 3.8 Schematic representation of stopped-flow apparatus. Syringes show the use of unbuffered cytochrome *c* syringe mixing with a second syringe of various buffers of different pH's. Reactions are monitored with a photomultiplier at 406 nm for changes in heme interaction.

pH Jump experiments were performed on WT and K72A Hu Cyt*c* using an Applied Photophysics apparatus shown in Figure 3.8. A two exponential equation for WT Hu Cytc was used at lower pH's based on residuals shown in Figure 3.9. The increase in conformational dynamics near the heme (monitored at 406 nm) is shown by the increase in curve steepness and decrease in reaction time as a function of final pH. Furthermore, Figure 3.9 shows that as pH increases above 10.00 a faster phase becomes present, shown in the bottom panel plots for pH 10.53 as higher order residuals become more appropriate fits.

For the two state model, rates and amplitudes were categorized by setting the fastest rate as $k_{obs}1$ with its respective amplitude being assigned as amplitude 1, A_1. The original interpretation used a two state model for WT and K72A Hu Cyt*c*. The fractional amplitude data in Figure 3.10 show what appears to be K72 binding (A; WT Hu Cyt*c*) by loss of amplitude upon mutation. In (B), a population of what we assigned to be K79 in K72A Hu Cyt*c* is seen whereas at higher pH in WT Hu Cyt*c* a decrease in amplitude is seen, corresponding with the fast phase where we hypothesized K72 binding. Data were fit as a function of pH for both WT and K72A Hu Cyt*c* and rate constants and amplitudes are shown in Table 3.3. Significant deviations are seen in the number of protons involved in the kinetic process from WT Hu Cyt*c* (2.3±0.18) to K72A Hu Cyt*c* (1.1±0.05), indicating the loss of lysine causes loss of a proton in the pH-jump. Furthermore in the transition itself we see a shift in the curve pK_{app} from (9.9±0.015) in WT Hu Cyt*c* to (9.5±0.02) in K72A Hu Cyt*c*.

This was our interpretation for quite some time until the data were revisited and fit with 3 and 4 exponential fits for WT Hu Cyt*c* and an additional 3 exponential fit for K72A Hu Cyt*c*. These residuals are shown in Figure 3.9 bottom panels. Three exponential fits are thus used instead shown as a summary in figure 3.11. This shows the main amplitude, A_2, being unchanged

compared to the original interpretation. However with A_2 we do see a corresponding decrease in $k_{obs,2}$. What our new interpretation adds that the original did not was the addition of a proline isomerization shown in our WT Hu Cyt*c* $A_3/k_{obs,3}$ data. Here we see a phase on a 0.1 s^{-1} timescale which disappears with the K72A mutation.

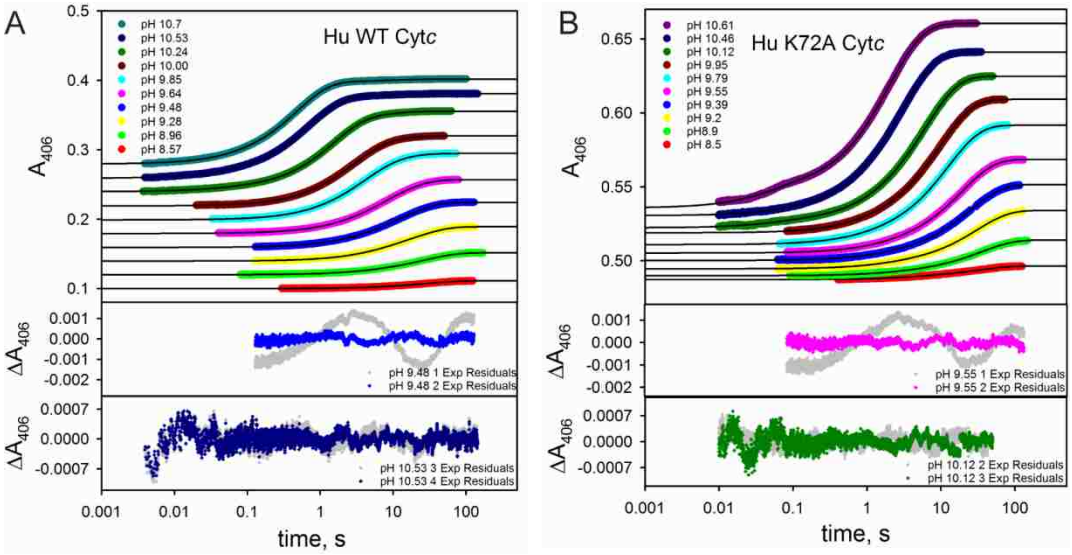

Figure 3.9 Stopped-flow data for upward pH jump experiments for WT Hu Cyt*c* (A) and K72A Hu Cyt*c* (B). The initial pH for all pH jumps experiments was pH 6. The final pH after mixing is indicated in the legend on each panel. From pH 8.57 to 9.48 for Hu WT Cyt*c* and from pH 8.5 to 9.95 for K72A Hu Cyt*c*, the solid curves are fits to a two-exponential equation. From pH 9.64 to 10.00 for Hu WT Cyt*c* and from pH 10.21 to 10.61 for K72A Hu Cyt*c*, the solid curves are fits to a three-exponential equation. From pH 10.24 to 10.7 for Hu WT Cyt*c*, the solid curves are fits to a four-exponential equation. The middle plot in panel A shows the residuals for a one (gray) versus a two (blue) exponential fit at pH 9.48 for WT Hu Cyt*c* data. The bottom plot in panel A shows the residuals for a three (gray) versus a four (dark blue) exponential fit at pH 10.53 for WT Hu Cyt*c* data. The middle plot in panel B shows the residuals for a one (gray versus a two (magenta) exponential fit for the pH 9.55 K72A Hu Cyt*c* data. The bottom plot in panel B shows the residuals for a two (gray) versus a three (dark green) exponential fit for the pH 10.12 K72A Hu Cyt*c* data. Some data traces in each plot have had a constant absorbance value added to all time points to so that all traces can be shown clearly in a single plot. All data were acquired at 25 ^{o}C.

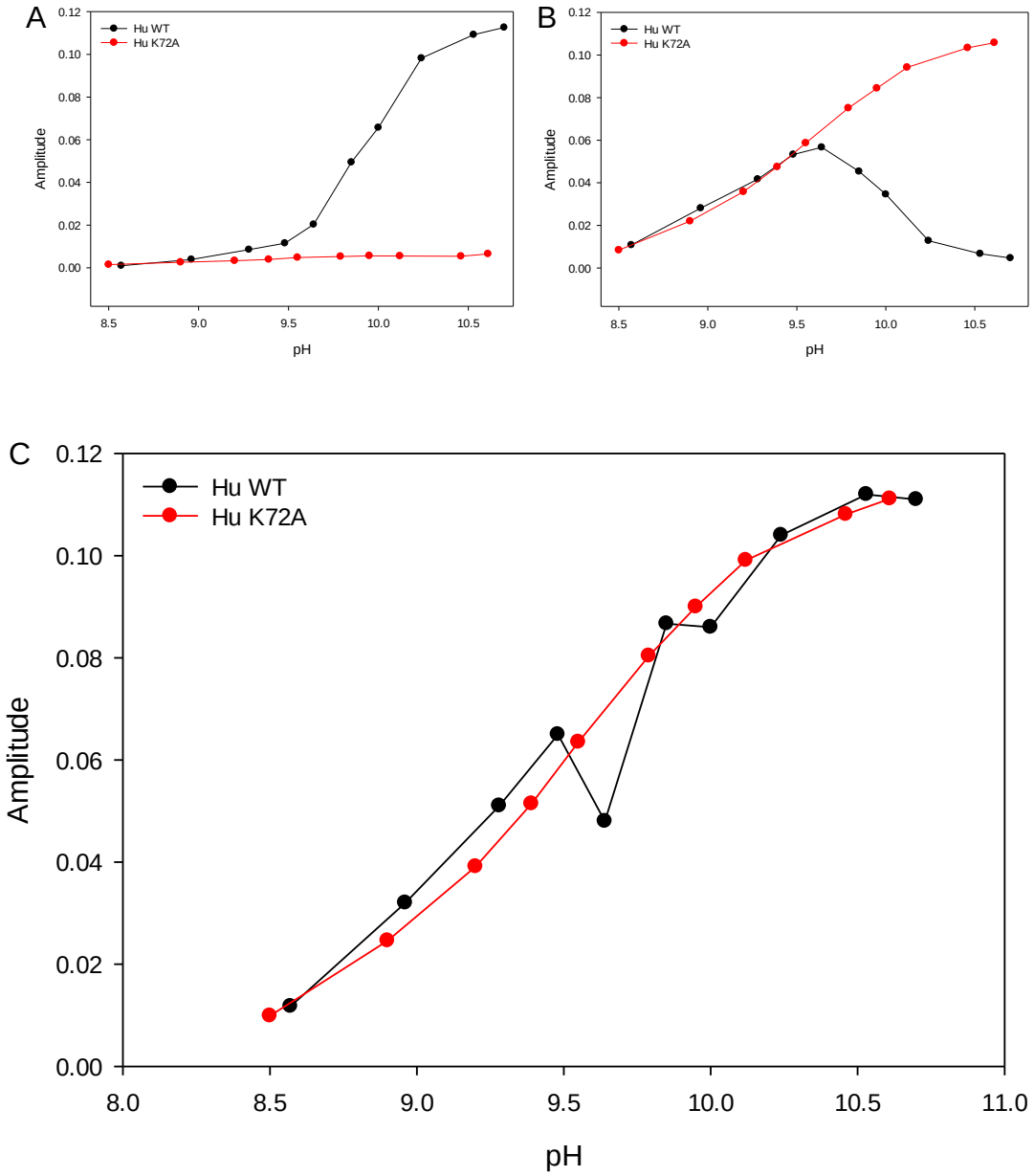

Figure 3.10 Fractional amplitude data of A_1 and A_2 upward pH Jump amplitudes for Hu WT and Hu K72A. This data is made by the addition of A_1 and A_2 for Hu WT and Hu K72A and subsequent fractionation of A_1 and A_2 into the total amplitude. Total Amplitude for fast phase data for the initial interpretation are shown in (A) whereas total amplitudes of slow phase data is shown in (B). (C) shows total amplitude data from Figure 3 corresponding to our current interpretation.

Table 3.3 The variables from the modified Henderson-Hasselbalch curve fits from Figure 3.10B.

Variant	A_N	A_{Alk}	n	pK_{app}
Hu WT	0.11±0.002	0.003±0.002	2.3±0.18	9.9±0.015
Hu K72A	0.11±0.002	0.001±0.002	1.1±0.05	9.5±0.02

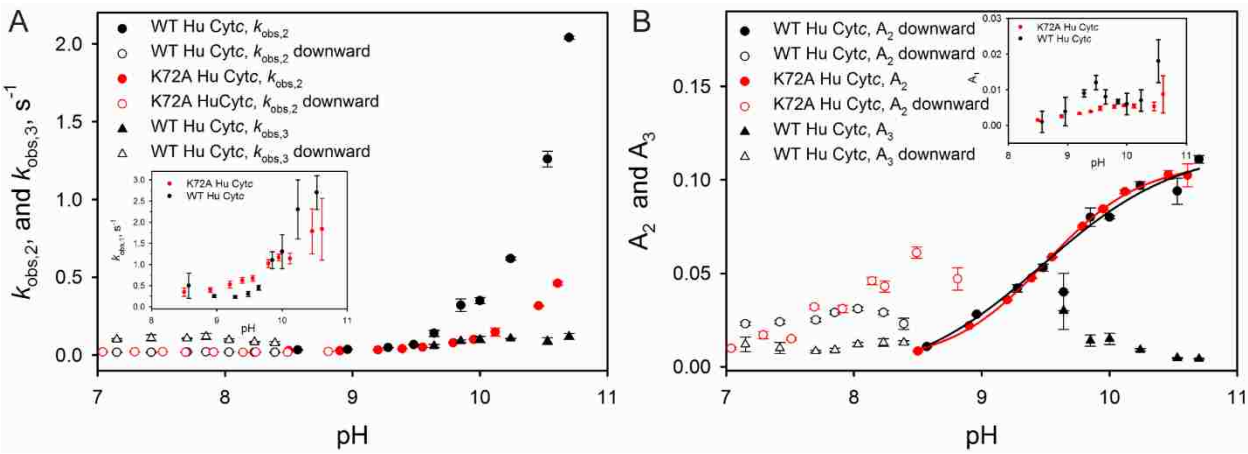

Figure 3.11 (A) Rate constants as a function of pH for the alkaline conformational transition of WT (black symbols) and K72A Hu Cyt*c* (red symbols). Data for a fast phase, $k_{obs,1}$, are shown in the inset. Data for two slower phases, $k_{obs,2}$ and $k_{obs,3}$, are shown as circles and triangles, respectively, in the main panel. (B) Amplitudes as a function of pH for the alkaline conformational transition of WT (black symbols) and K72A Hu Cyt*c* (red symbols). Data for the fast phase amplitude, A_1, are shown in the inset. Two slower phases, A_2 and A_3, are shown as circles and triangles, respectively, in the main panel. The solid curves are fits of the A_2 versus pH data for WT (black) and K72A (red) Hu Cyt*c* to the Henderson-Hasselbalch equation (eq 2.2 in Experimental Procedures). Rate constants and amplitudes obtained from upward pH jump experiments are shown as solid symbols and for downward pH jump experiments as open symbols. Upward jumps had an initial pH of 6.0 and downward jumps had an initial pH of near 10. Data were acquired at 25 ^{o}C. Final buffers after mixing were 10 mM with 100 mM NaCl. Final protein concentration was 10 μM. Error bars are standard deviations.

F. Peroxidase Activity

Peroxidase activity was investigated for Hu WT and Hu K72A cyt*c*. The reaction used is shown in Figure 3.12. It uses guaiacol and hydrogen peroxide which is catalyzed by cytochrome *c* to form the molecule tetraguaiacol and water, the reaction can be monitored at 470 nm for tetraguaiacol formation. Previous investigations have worked with yeast iso-1-Cyt*c* which contains a trimethylated lysine at position 72, tmK72, and lacks the need to regulate peroxidase activity because there is no apoptotic pathway in yeast. Working with K72A variants in yeast iso-1-Cyt*c* showed not only increased peroxidase activity, but an increase in access to alternative conformers (McClelland *et al* 2014).

Figure 3.13 shows representative Michaelis-Menten plots for WT and K72A Hu Cyt*c* peroxidase activity. 3.14A shows K_m values for Hu WT and Hu K72A. These values indicate that

the interaction between Guaiacol and Cyt*c* whether Hu WT or Hu K72A remains unchanged over the entire tested pH regime. However, looking at catalytic efficiency we see a significant increase in k_{cat} over a region of physiological pH's for Hu K72A over those of Hu WT. This observation provides evidence that one possible reason for human evolution of the K72 residue is to regulate peroxidase activity in humans. The values for these fits are shown in Table 3.5.

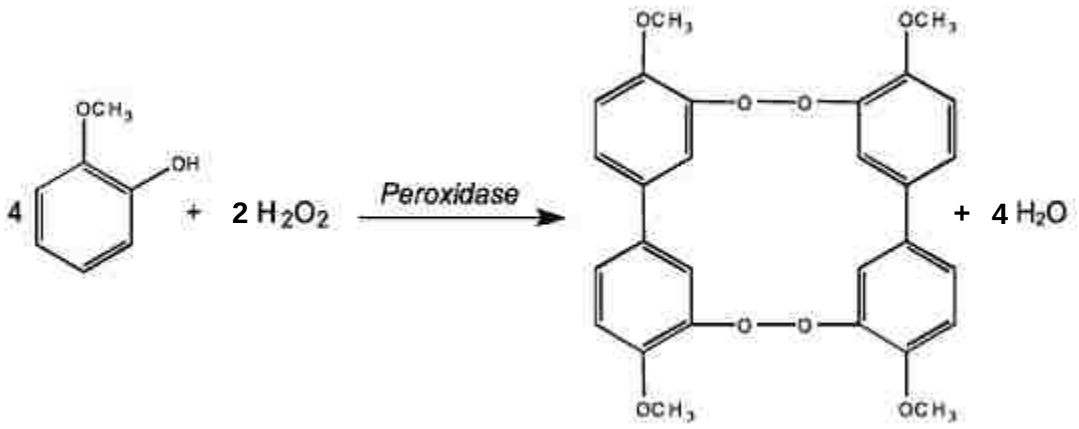

Figure 3.12 Schematic representation of the formation of tetraguaiacol from guaiacol and hydrogen peroxide. This reaction is catalyzed by cytochrome c and monitored at 470 nm for the formation of tetraguaiacol.

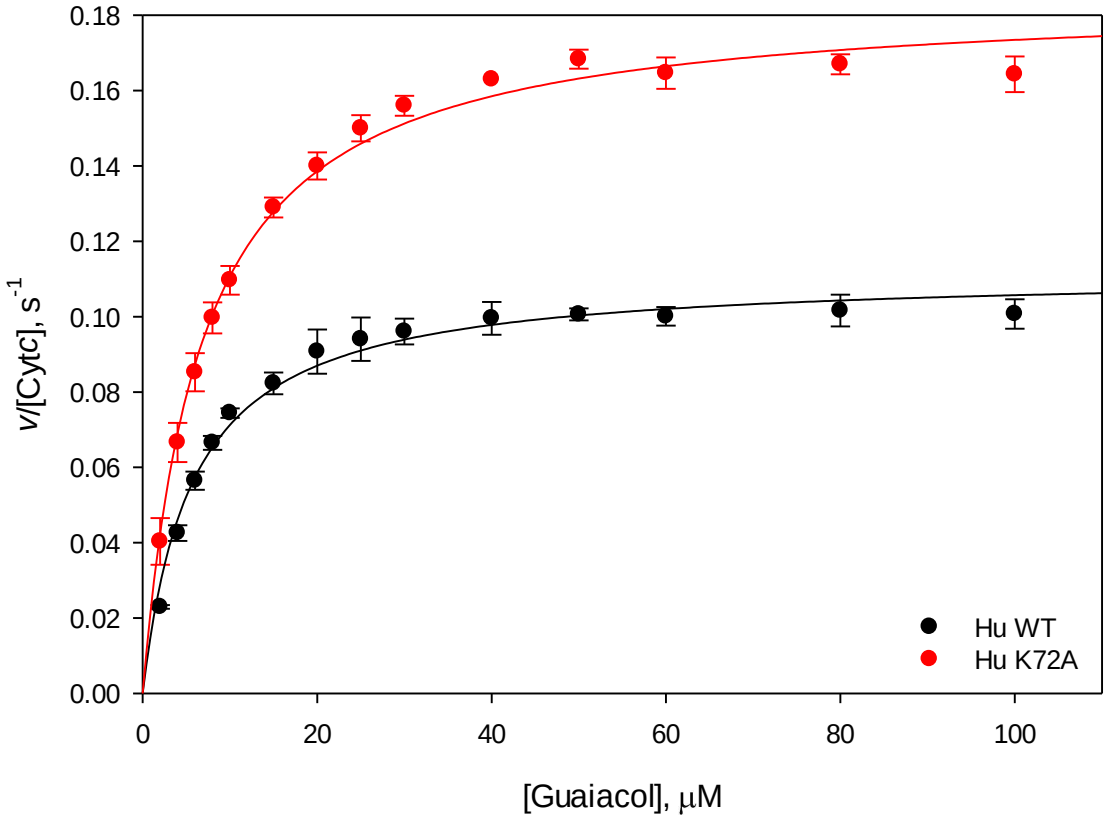

Figure 3.13 Peroxidase activity of Hu WT (black) and Hu K72A (red) Cyt*c* at pH 7. Curves are fits to Michaelis-Menten equation (Equation 2.7). Data was taken at 25 °C in 10 mM buffer with 100 mM NaCl.

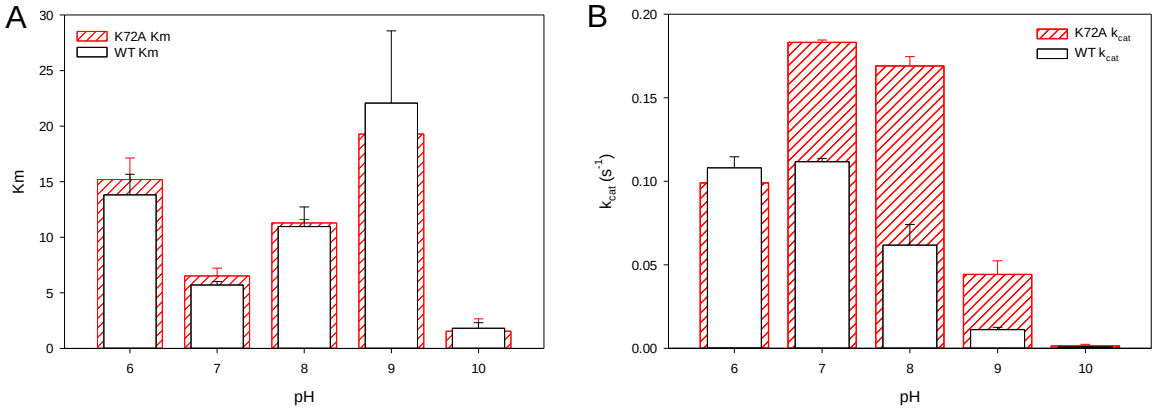

Figure 3.14 Data taken from Michaelis-Menten fits of Hu WT (white bars black outline) and Hu K72A (red outlined bars with slashes) Cyt*c* with K_m (A) and k_{cat} values (B) being shown. Error bars are the standard deviations of triplicate experiments for each pH unit. Data were taken at 25 °C in 10 mM buffer with 100 mM NaCl.

Table 3.4 K_m and k_{cat} values for Hu WT and Hu K72A as a function of pH.

pH	K_m (M)		k_{cat} (s^{-1})	
	WT	K72A	WT	K72A
6.0	14±2	15±2	0.108±0.007	0.099±0.008
7.0	5.7±0.3	6.5±0.7	0.112±0.002	0.183±0.001
8.0	11±2	11.3±0.3	0.06±0.01	0.169±0.006
9.0	22±7	19±2	0.011±0.001	0.044±0.008
10.0	1.8±0.5	2±1	0.0008±0.0002	0.0024±0.0008

G. Discussion

The crystal structure overlay which we present here in figure 3.1 shows that with the K72A mutation there is little difference in structure compared to that of Hu WT. When looking at the global stability of the proteins we also see from the unfolding midpoint, C_m (M), is only slightly stabilized for the K72A variant from 2.55±0.01 in Hu WT to 2.75±0.03 in that of Hu K72A.

Investigation into the alkaline transition by monitoring the charge transfer band for Hu WT and Hu K72A Cyt*c* shows that there is a clear stabilization in the titration curves for Hu K72A, which is shown by shifts in $pK_{a(apps)}$ of Hu WT which is 9.54±0.03 to that of Hu K72A which is 10.00±0.13. One hypothesis for the observation of this alkaline transition shift is such that if the local concentration of alkaline state residues has been decreased, the native ligand (M80-heme) would be more favorable because the alternative alkaline conformations would be disfavored to an extent. However, a more accurate interpretation is suggested by the kinetic data.

Kinetic data discussed here clearly shows a two or more exponential model more accurately fits the data than the single exponential model for upward pH- jumps which has been used in the past (Ying *et al* 2009). Residuals shown in figure 3.8 show the distinct improvement in the fit. Both $k_{obs,1}$ and $k_{obs,2}$ rates are consistent with what is expected in the alkaline transition (Figure 3.7) in both Hu WT and K72A Cyt*c*. This indicates that the model previously discussed that K72 plays a significant role as a ligand in the alkaline transition is likely untrue. Previous work shows a coupled proline isomerization to the formation of a His73-heme alkaline conformer of yeast iso-1-Cyt*c* (Martinez and Bowler 2004). We assign the primary alkaline conformer (A_2, $k_{obs,2}$) to this K73-mediated alkaline conformer of Hu Cyt*c*.

The primary impetus for this work was to determine if the enhancement of peroxidase activity observed for yeast iso-1-Cyt*c* upon introduction of the K72A mutation also occurs with

Hu Cyt*c*. The pH dependence of k_{cat} for WT versus K72A Hu Cyt*c* is similar to our previous observations for yeast iso-1-Cyt*c*. At pH 6, k_{cat} is identical for the WT proteins and the K72A variants of both yeast iso-1-Cyt*c* and Hu Cyt*c*. However, at pH 7 and above k_{cat} is significantly higher for the K72A variants of yeast and human Cyt*c*. For yeast iso-1-Cyt*c*, the K72A mutation leads to a 30% increase in k_{cat}, whereas for Hu Cyt*c* a 60% increase is observed. At pH 8, a two-fold increase in k_{cat} results from the K72A mutation, whereas a three-fold increase is observed for Hu Cyt*c*. Thus, Lys72 is also important in suppressing the basal peroxidase activity of Hu Cyt*c*. However, the percent increase in activity is larger for Hu Cyt*c* than for yeast iso-1-Cyt*c*.

The decrease in k_{cat} as pH increases (Figure 3.14B) is also observed for horse Cyt*c* (Diederix *et al* 2001; Radi *et al* 1991) and has been attributed to replacement of Met80 by a lysine, which is a stronger ligand for Fe(III) than methionine. At pH 7 and 8, the alkaline conformer for both WT and K72A Hu Cyt*c* is poorly populated (Figure 3.6) and thus is not a significant factor in the pH regime where the largest enhancement of peroxidase activity is observed for the K72A variant relative to WT Hu Cyt*c* (Figure 3.14B). Based on the horse Cyt*c* (Figure 3.2A) and yeast iso-1-Cyt*c* structure, we have suggested that Lys72 may act like a brace across Ω-loop D, stabilizing it against opening and allowing reactive oxygen species like hydrogen peroxide to bind to the heme iron (McClelland *et al* 2014). The human Cyt*c* structure indicates that this interaction of Lys72 with the other side of Ω-loop D may not be the primary reason that Lys72 inhibits the intrinsic peroxidase activity of Cyt*c*. In fact, the water-mediated hydrogen bond network that connects one-side of Ω-loop D with the other is similar in WT and K72A Hu Cyt*c* (Figures 3.2 B and C). In our structure of K72A iso-1-Cyt*c*, (McClelland *et al* 2014) where Met80 ligation to the heme is replaced by a hydroxide, the smaller side chain at position 72 appears to be essential for allowing the backbone movement necessary for expulsion

of Met80 from the heme crevice. Thus, the primary function of Lys72 may be to sterically inhibit this backbone motion, suggesting that any amino acid of sufficient steric size at position 72 would reduce the intrinsic peroxidase activity of cytochrome *c*. Our K72A iso-1-Cytc structure shows that the side chain of residue 81 must move toward Lys72 to allow expulsion of Met80 from the heme crevice (McClelland *et al* 2014). Yeast iso-1-Cyt*c* has alanine at this position and Hu Cytc has isoleucine at this position. The larger percent increase in k_{cat} for the K72A mutation for Hu Cyt*c* versus yeast iso-1-Cyt*c* may result from the greater steric congestion of isoleucine at position 81 of Hu Cyt*c* versus alanine at this position for yeast iso-1-Cyt*c*.

To keep the current results in context, we note that the basal peroxidase activity of WT Hu Cyt*c* is about 15% less than horse Cyt*c* at pH 7 under the same conditions. The K72A mutation leads to a 1.6-fold increase in k_{cat}, whereas formation of a domain-swapped dimer of horse Cyt*c* produces a 5-fold increase in k_{cat} (Wang *et al* 2011). Both mammalian proteins have a k_{cat} that is 20-fold less than that of the yeast iso-1-Cyt*c*. Thus, while Lys72 plays a role in modulating peroxidase activity in both yeast and mammalian cytochromes *c*, evolution of other segments of the primary structure of cytochrome *c* are responsible for the substantial suppression of the basal peroxidase activity of Cyt*c* in higher eukaryotes.

H. Conclusions

Lys72 is a significant suppressor of peroxidase activity in both yeast and human cytochromes *c*. The percent effect of Lys72 is somewhat larger in human cytochrome *c*. The K72A mutation causes a small increase in global stability, thus the intrinsic peroxidase activity of cytochrome *c* must not be solely controlled by global stability. Structural data for horse and yeast cytochromes *c* suggested that Lys72 stabilizes Ω-loop D via direct interactions with the far side of Ω-loop D. The crystal structures of WT Hu Cyt*c* and of the K72A variant indicate that Lys72 may not be the primary mediator of interactions between opposite sides of Ω-loop D. Instead, it appears that steric clashes between the side chains of positions 72 and 81 may be of primary importance in suppressing Ω-loop D dynamics that support peroxidase activity. This interpretation is supported by our crystal structure of K72A iso-1-Cyt*c* with Met80-heme ligation replaced by heme-hydroxide ligation which requires the side chain of position 81 to move against that of residue 72 (McClelland *et al* 2014). Our observation that the percent enhancement of peroxidase activity by the K72A mutation is larger for Hu Cyt*c* which has isoleucine at position 81 than for yeast iso-1-Cyt*c* which has alanine at position 81 supports this interpretation.

Chapter 4
Evolution of Alanine to Isoleucine at position 81 in the Heme Crevice Loop in Human Cytochrome *c*

A. Introduction of I81A Hu Cyt*c*

Only three residues within the heme crevice loop are not universally conserved. These are those at positions 81, 83, and 85. Here I investigate the residue at position 81 which is an alanine in yeast iso-1-Cyt*c* and isoleucine in human Cyt*c*. Previously, data have shown significant movement in A81 when M80 is displaced from the heme (McClelland *et al* 2014). Furthermore, the more sterically demanding residue, isoleucine, has evolved in mammalian cytochrome *c*. Here we hypothesize that mammalian cytochromes *c* evolved this mutation to minimize peroxidase activity compared to yeast iso-1-Cyt*c*.

B. Global Unfolding Thermodynamics of I81A Hu Cyt*c*

GdnHCl unfolding experiments monitored by CD were performed on Hu WT and Hu I81A Cyt*c*. As indicated by Figure 4.1, a small destabilization of the native conformer is seen in the I81A variant. The m-values, $\Delta G_u^{o'}(H_2O)$, and C_m values shown Table 4.1 show that C_m increases slightly, but the *m*-value decreases significantly, with a decrease in global stability and $\Delta G_u^{o'}(H_2O)$ of roughly 0.5 kcal/mol. As stated in the previous chapter with the Hu K72A Cyt*c* variant, changes within the global stability of a protein are often small with single variant mutations.

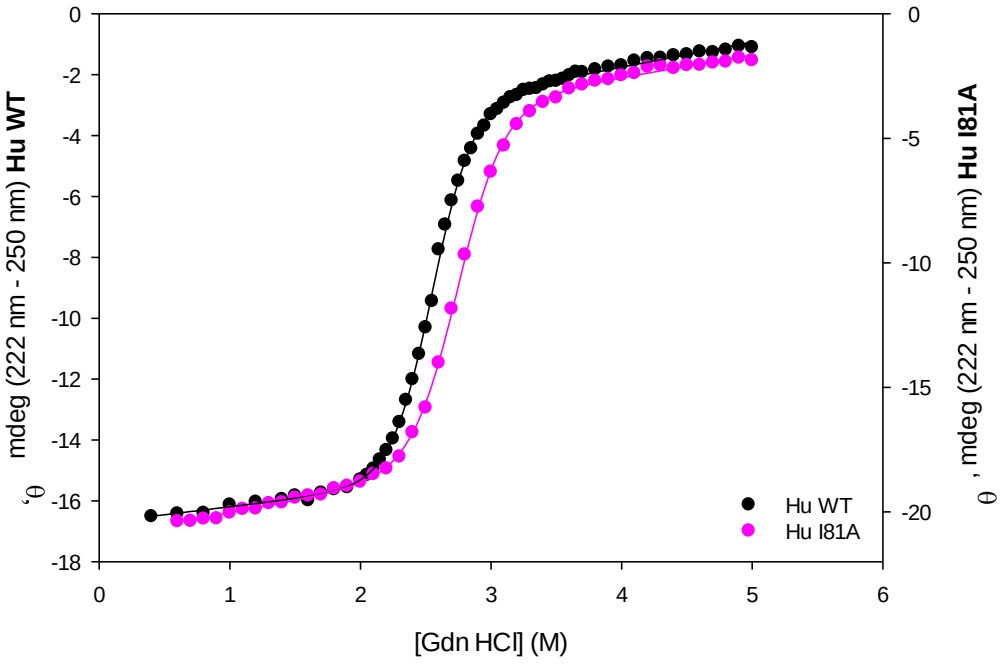

Figure 4.1 Overlay of Gdn HCl denaturation curves of Hu WT and Hu I81A Cyt*c*. Y-axes align to indicated curve. The curves shown in this figure are fits to Equation 2.1 with parameters obtained being listed in Table 4.1.

Table 4.1 Guanidine Denaturation values for Hu WT and Hu I81A variants

Variant	m(kcal $mol^{-1}M^{-1}$)	$\Delta G_u^{o'}(H_2O)$ (kcal mol^{-1})	C_m
Hu WT	3.71±0.05	9.46±0.11	2.55±0.01
Hu I81A	3.29±0.06	8.85±0.31	2.69±0.05

Hu I81A shows minor changes in $\Delta G_u^{o'}(H_2O)$ from that of Hu WT (9.46±0.11 kcal mol^{-1}). These data taken indicate that no major global stability structural changes occur due to this mutation. A decrease in cooperativity (*m*-value) is seen to lead to a decrease in overall protein stability.

C. Alkaline Conformational Transition Thermodynamics of I81A Hu Cyt*c*

pH titrations were performed on I81A Hu Cyt*c* to compare with the previous results of WT Hu Cyt*c*. First addressing Hu I81A Cyt*c*, data in figure 4.2B shows a clear destabilization on the native conformer relative to the alkaline conformer compared to Hu WT Cyt*c* with the measured $pK_{a(app)}$ decreasing by 0.5 unit (Table 4.2). Figure 4.2A shows Overlays of all three repeats of alkaline pH titrations as well as an acid pH titration for Hu I81A Cyt*c*.

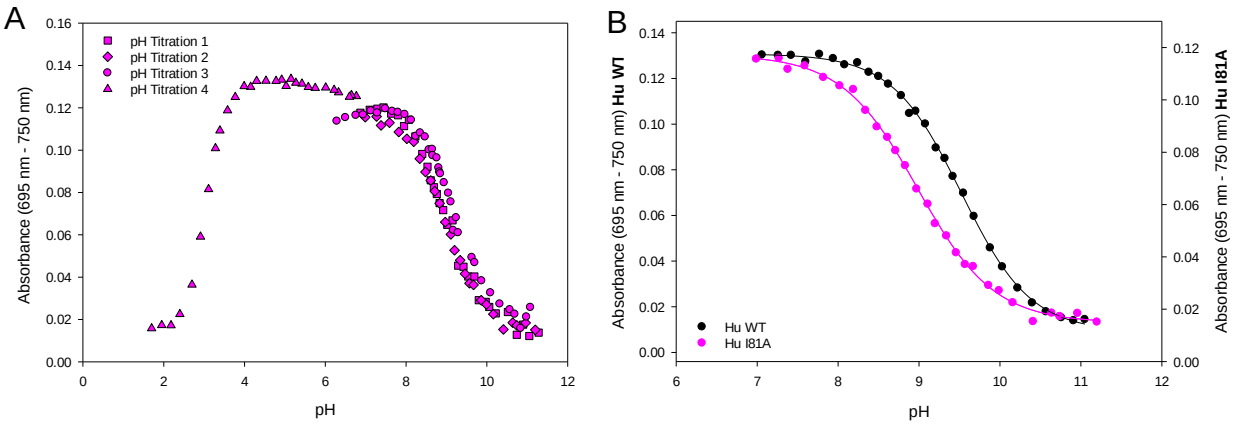

Figure 4.2 Triplicate individual pH titrations of Hu I81A Cyt*c* showing the alkaline conformational transition (Titrations 1-3) and the acidic pH titration (Titration 4) (A). (B) shows single plots of Hu WT and Hu I81A Cyt*c*.

Table 4.2 pH Titration values for Hu WT and Hu I81A

Variant	$pK_{a(app)}$	n
WT	9.53±0.03	1.04±0.025
I81A	9.05±0.12	0.94±0.06

The n value, or number of protons, involved in the process is also included in table 4.2. Both WT and I81A Hu Cyt*c* undergo the alkaline transition as a single proton processes.

D. Alkaline Conformational Transition Kinetics

Stopped-Flow pH Jumps were performed on I81A Hu Cyt*c* for comparison with WT Hu Cyt*c* (Chapter 3). Figure 4.3 A shows stacked plots for I81A Hu Cyt*c* and curve residuals show a large deviation between double and triple exponential fits whereas residuals in B show only minor residual differences between triple and quadrupole exponential fits. These residuals show that the best model to use for I81A Hu Cyt*c* is the three exponential model.

Total amplitudes shown in figure 4.4 have a similar destabilization for I81A Hu Cyt*c* as previously seen in our equilibrium data (Figure 4.2 B). The individual rates and amplitudes are shown in figure 4.5. Fast phase rate data, $k_{obs,1}$, show a constant phase throughout nearly the entire pH regime which is consistent with what has been seen before in yeast iso-1-Cyt*c* (Bandi and Bowler 2012). $k_{obs,2}$ data show stable rate constants throughout the low pH regime with significant growth above pH 10, a greater increase in rate than $k_{obs,3}$. This is consistent with what is seen in both WT and K72A Hu Cyt*c* (Figure 3.10). A_1 shows growth of fast phase data throughout the pH regime, whereas A_2 shows a significant population with increasing pH. A_3 increases much earlier in the pH regime and decreases to lower amplitude, matching with what we determine to be a proline isomerization at high pH.

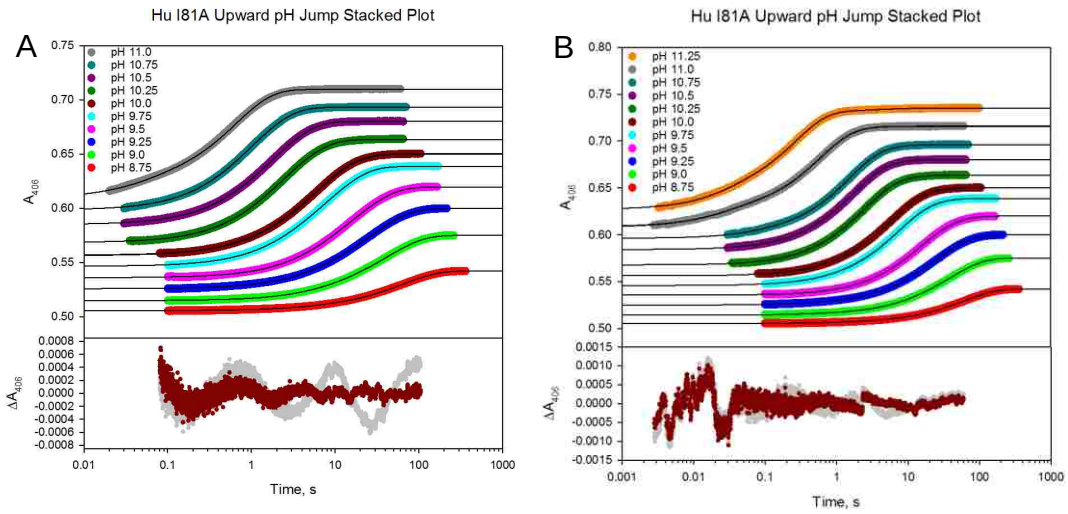

Figure 4.3 Stopped-flow stacked plots for upward jumps of I81A Hu Cyt*c*. (A) shows pH jump data with corresponding fits (black lines). The bottom panel shows double exponential residuals (grey) and triple exponential residuals (maroon) for I81A Hu Cyt*c* at pH 10.00. (B) shows similar data with extended regions at higher pH regime and fit with triple exponential residuals (grey) and quadruple exponential residuals (maroon) for I81A Hu Cyt*c* at pH 11.00. Initial pH of protein was pH 6 whereas the final pH is indicated by colored plots and figure legends. Data was acquired at 25°C.

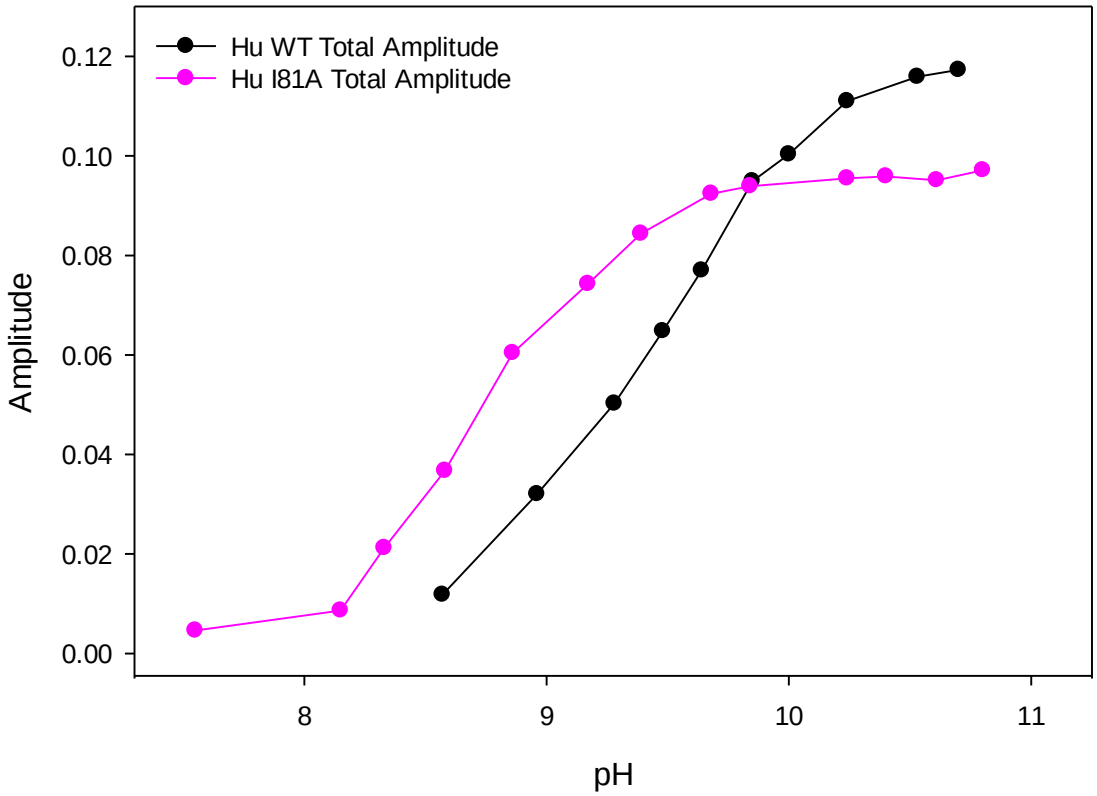

Figure 4.4 Total amplitudes of Hu WT (Black) and Hu I81A (Pink). Hu WT Cyt*c* is the sum of two exponential fits (A_1+A_2) whereas Hu I81A Cyt*c* is the sum of three exponential fits (A_1+A_2+A_3).

\

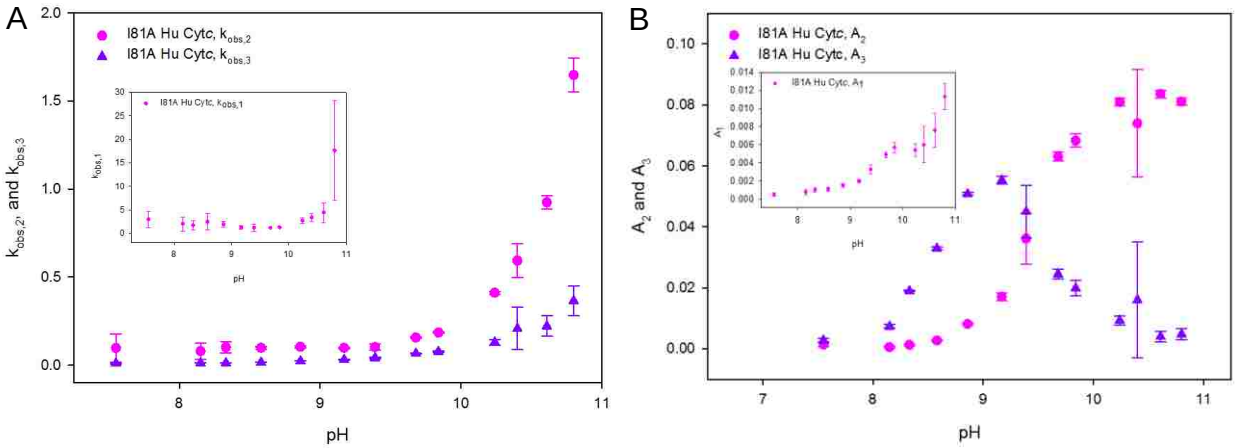

Figure 4.5 Upward pH jump rates for I81A Hu Cyt*c* showing $k_{obs,1}$ (inset; pink) $k_{obs,2}$ (pink) and $k_{obs,3}$ (purple) are shown in (A). Upward pH jump amplitudes for I81A Hu Cyt*c*, A_1 (inset; pink), A_2 (pink), and A_3 (purple) are shown in (B). pH jumps had an initial pH of 7.0 and data was acquired at 25.0°C. Final buffers after mixing were 10 mM with 100 mM NaCl. Final protein concentration was 10 µM. Error bars are standard deviations. Solid curves are fits to the Henderson-Hasselbalch equation (Equation 2.2).

E. Peroxidase Activity

Peroxidase Activity was monitored for Hu WT and Hu I81A Cyt*c*. The reaction used in this experiment was shown previously in Figure 3.12 from Chapter 3. Experiments were performed in triplicate and the average and standard deviations of each with respect to pH were used for peroxidase activity data. Figure 4.6 shows an example Michaelis-Menten plot for Hu I81A at pH 7.0. k_{cat} and K_m values for the entire pH regime are shown in Figure 4.7 (their values are collected in Table 4.3).

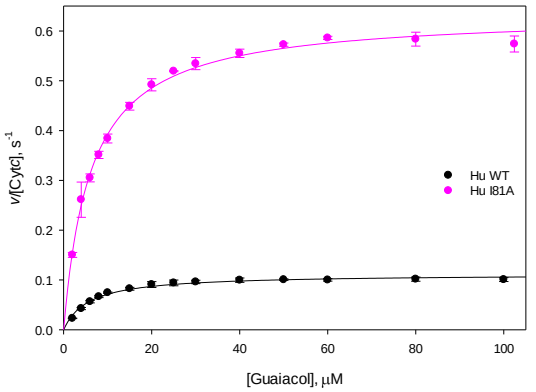

Figure 4.6 Peroxidase activity of Hu WT (black) and Hu I81A (Pink) Cyt*c* at pH 7. Curves are fits to Michaelis-Menten equation (equation 2.7). Data was taken at 25 °C in 10 mM buffer with 100 mM NaCl.

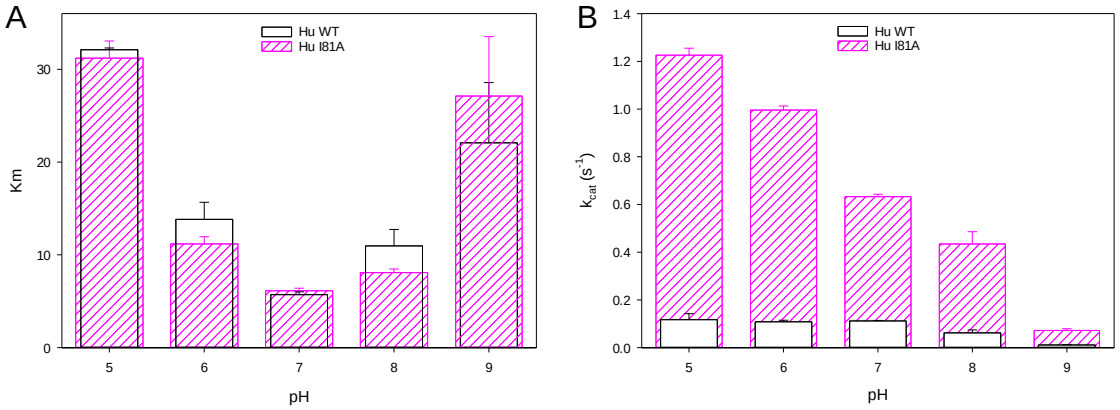

Figure 4.7 Parameters taken from Michaelis-Menten fits of Hu WT (white bars black outline) and Hu I81A (pink outlined bars with slashes) Cyt*c* with Km (A) and k_{cat} values (B) being shown. Error bars are the standard deviations of triplicate experiments for each pH. Data were taken at 25 °C in 10 mM buffer with 100 mM NaCl.

Table 4.3 K_m and k_{cat} values WT and I81A Hu Cyt*c*

pH	K_m (M)		k_{cat} (s^{-1})	
	WT	I81A	WT	I81A
5.0	32±2	31±2	0.11±0.03	1.2±0.03
6.0	14±2	11±0.1	0.108±0.007	1.0±0.02
7.0	5.7±0.3	6.1±0.3	0.112±0.002	0.63±0.01
8.0	11±2	8.1±0.4	0.06±0.01	0.43±0.05
9.0	22±7	29±9	0.011±0.001	0.07±0.005

F. Discussion

Here WT and I81A Hu Cyt*c* are used to look at changes in the heme crevice loop region upon loss of I81. Global unfolding thermodynamics show a minor destabilization, with a shift in $\Delta G_u^{o'}(H_2O)$ of 0.14 M in I81A compared to WT Hu Cyt*c*. Investigation of the alkaline conformational transition shows a significant destabilization in I81A compared to WT Hu Cyt*c*, with a shift in $pK_{a(app)}$ of 0.48 compared to that of WT.

Investigation of kinetics data show a similar trend in pH shift, with medium and fast phase amplitudes (Figure 4.5 C and E) I81A compared to WT Hu Cyt*c*. Investigation of WT and I81A Hu Cyt*c* peroxidase activity show that Km values are similar across all pH's for both cytochromes *c*. However, I81A k_{cat} values are significantly higher than those of WT Hu Cyt*c*, decreasing in value as pH becomes more alkaline.

G. Conclusions

A Hu I81A Cytc variant was made to investigate the significance of residue movement seen upon displacement of the natively bound M80-heme ligand and its contribution to peroxidase activity (McClelland *et al* 2014). The local unfolding alkaline conformational transition shows a destabilization in support of our hypothesis as loss of M80-heme ligation happens earlier in the pH transition, hypothetically allowing for such peroxidase activity to take place.

Kinetic data show a destabilized I81A variant compared to Hu WT Cyt*c* in both significant phases (Figure 4.5 C and E), with similar reasoning to that of the previously mentioned alkaline pH transition.

Lastly, investigation of peroxidase activity, specifically the significant increase in k_{cat} values of I81A, confirm our hypothesis that the evolution of isoleucine to alanine in Hu Cyt*c* may have taken place to elevate the peroxidase activity seen in yeast iso-1-cyt*c*.

References

Adams, P. D., Afonine, P. V., Bunkóczi, G., Chen, V. B., Davis, I. W., Echols, N., Headd, J. J., Hung, L.-W., Kapral, G. J., Grosse-Kunstleve, R. W., McCoy, A. J., Moriarty, N. W., Oeffner, R., Read, R. J., Richardson, D. C., Richardson, J. S., Terwilliger, T. C., and Zwart, P. H. (2010) PHENIX: a comprehensive Python-based system for macromolecular structure solution, *Acta Crystallogr., Sect. D: Biol. Crystallogr. 66*, 213-221.

Afify M., Refaat R.K., Elhosary Y.A., Abdelfattah E.H., Fahim H.H., and Ezzat W. M.; The Possible role of Cytochrome c and programmed cell death protein 4 (PDCD4) on pathogenesis of hepatocellular carcinoma *Journal of Genetic Engineering and Biotechnology* 13(2015):157-163.

Amino Acid Sequences in Cytochrome-*c* proteins from 20 different species. Adapted from Strahler, A; *Science and Earth History* (1987): 348.

Anfinsen C.B.; Principles that Govern the Folding of Protein Chains *Science* 181.4096 (1973): 223-230.

Bandi S., Baddam., S., and Bowler B.E.; Alkaline conformational transition and gated electron transfer with a Lys 79 →His variant of iso-1-cytochrome *c Biochemistry* 46.37(2007):10643-54

Bandi S., Bowler, B.E.; (2012) A Cytochrome c Electron Transfer Switch Modulated by Heme Ligation and Isomerization of a Peptidyl-Prolyl Bond *Peptide Science* 100.1, 114-124.

Berghuis, A. M., and Brayer, G. D. (1992) Oxidation state-dependent conformational changes in cytochrome *c*, *J. Mol. Biol. 223*, 959-976.

Bushnell, G. W., Louie, G. V., and Brayer, G. D. (1990) High-resolution three-dimensional structure of horse heart cytochrome *c*, *J. Mol. Biol. 214*, 585-595.

Cherney, M. M., Junior, C. C., Bergquist, B. B., and Bowler, B. E. (2013) Dynamics of the His79-heme alkaline transition of yeast iso-1-cytochrome *c* probed by conformationally gated electron transfer with Co(II)bis(terpyridine), *J. Am. Chem. Soc. 135*, 12772-12782.

Cherney, M. M., Junior, C., and Bowler, B. E. (2013) Mutation of trimethyllysine-72 to alanine enhances His79-heme mediated dynamics of iso-1-cytochrome *c*, *Biochemistry 52*, 837-846.

Diederix, R. E. M., Ubbink, M., and Canters, G. W. (2001) The peroxidase activity of cytochrome *c*-550 from *Paracoccus versutus*, *Eur. J. Biochem. 268*, 4207-4216.

Emsley, P., Lohkamp, B., Scott, W. G., and Cowtan, K. (2010) Features and development of Coot, *Acta Crystallogr., Sect. D: Biol. Crystallogr. 66*, 486-501.

Gabr S.A., and Al-Ghadir A.H.; Role of cellular oxidative stress and cytochrome *c* in the pathogenesis of psoriasis *Archives of Dermatological Research* 304(2012):451-457.

Goldes M.E., Jeakins-Cooley M.E., McClelland L.J., Mou T-C., Bowler B.E.; Disruption of a hydrogen bond network in human versus spider monkey cytochrome *c* affects heme crevice stability *Journal of Inorganic Chemistry* 158(2016):62-69.

Goldschmid, O. (1953) The effect of alkali and strong acid on the ultraviolet absorption spectrum of lignin and related compounds, *J. Am. Chem. Soc. 75*, 3780-3783.

Haber, E., and Anfinsen C.B.; Side-chain Interactions Governing the Pairing of Half-cysteine Residues in Ribonuclease* *The Journal of Biological Chemistry* 237.6 (1962): 1839-1844.

Hong, X., and Dixon, D. W. (1989) NMR study of the alkaline isomerization of ferricytochrome *c*, *FEBS Lett. 246*, 105-108.

Kokhan O., Wraight C.A., and Taljhorshid E.; The Binding Interface of Cytochrome *c* and Cytochrome c_1 in the bc_1 Complex: Rationalizing the Role of Key Residues *Biophysical Journal* 99(2010):2647-2656.

Kristinsson, R., and Bowler, B. E. (2005) Communication of stabilizing energy between substructures of a protein, *Biochemistry 44*, 2349-2359.

Levinthal, C. Are there pathways for protein folding? *J. Chim. Phys.* 65, 44-45 (1968).

Maity H., Rumbley J N., and Englander S.W.; Functional Role of a Protein Foldon-An Ω-Loop Foldon Controls the Alkaline Transition in Ferricytochrome c *Proteins* 63(2006):349-355.

Martinez, R. E., and Bowler, B. E. (2004) Proton-mediated dynamics of the alkaline conformational transition of yeast iso-1-cytochrome *c*, *J. Am. Chem. Soc. 126*, 6751-6758.

McClelland, L. J., Mou, T.-C., Jeakins-Cooley, M. E., Sprang, S. R., and Bowler, B. E. (2014) Structure of a mitochondrial cytochrome *c* conformer competent for peroxidase activity, *Proc. Natl. Acad. Sci. U.S.A. 111*, 6648-6653.

Moore, G. R., and Pettigrew, G. W. (1990) *Cytochromes c: Evolutionary, Structural and Physicochemical Aspects*, Springer-Verlag, New York.

Nelson, C. J., and Bowler, B. E. (2000) pH dependence of formation of a partially unfolded state of a Lys 73 -> His variant of iso-1-cytochrome *c*: implications for the alkaline conformational transition of cytochrome *c*, *Biochemistry 39*, 13584-13594.

Nelson D. P., and Kiesow L. A.; Enthalpy of decomposition of hydrogen perodide by catalase at 20 degrees C (with molar extinction coefficients with H_2O_2 solutions in the UV) *Journal of Analytical Biochemistry* 49.2(1972): 474-8

Noble, R. W., and Gibson, Q. H. (1970) The reaction of ferrous horseradish peroxidase with hydrogen peroxide, *J. Biol. Chem. 245*, 2409-2413.

Nozaki, Y. (1972) The preparation of guanidine hydrochloride, *Methods Enzymol. 26*, 43-50.

Olteanu, A., Patel, C. N., Dedmon, M. M., Kennedy, S., Linhoff, M. W., Minder, C. M., Potts, P. R., Deshmukh, M., and Pielak, G. J. (2003) Stability and apoptotic activity of recombinant human cytochrome *c*, *Biochem. Biophys. Res. Commun. 312*, 733-740.

Otwinowski, Z., and Minor, W. (1997) Processing of X-ray diffraction data collected in oscillation mode, *Methods Enzymol. 276A*, 307-326.

Pace, C. N., Shirley, B. A., and Thomson, J. A. (1989) Measuring the conformational stability of a protein, In *Protein structure: a practical approach* (Creighton, T. E., Ed.), pp 311-330, IRL Press at Oxford University Press, New York.

Patel, C. N., Lind, M. C., and Pielak, G. J. (2001) Characterization of horse cytochrome *c* expressed in *Escherichia coli*, *Protein Expression Purif. 22*, 220-224.

Pollock, W. B., Rosell, F. I., Twitchett, M. B., Dumont, M. E., and Mauk, A. G. (1998) Bacterial expression of a mitochondrial cytochrome *c*. Trimethylation of Lys72 in yeast iso-1-cytochrome *c* and the alkaline conformational transition, *Biochemistry 37*, 6124-6131.

Radi, R., Thomson, L., Rubbo, H., and Prodanov, E. (1991) Cytochrome *c*-catalyzed oxidation of organic molecules by hydrogen peroxide, *Arch. Biochem. Biophys. 288*, 112-117.

Rajagopal, B. S., Edzuma, A. N., Hough, M. A., Blundell, K. L. I. M., Kagan, V. E., Kapralov, A. A., Fraser, L. A., Butt, J. N., Silkstone, G. G., Wilson, M. T., Svistunenko, D. A., and Worrall, J. A. R. (2013) The hydrogen-peroxide-induced radical behaviour in human cytochrome *c*–phospholipid complexes: implications for the enhanced pro-apoptotic activity of the G41S mutant, *Biochem. J. 456*, 441-452.

Redzic, J. S., and Bowler, B. E. (2005) Role of hydrogen bond networks and dynamics in positive and negative cooperative stabilization of a protein, *Biochemistry 44*, 2900-2908.

Ross C.A., and Poirier M.A.; Protein aggregation and neurodegenerative disease *Nature Medicine* (2004): S10-S17.

Rosell, F. I., and Mauk, A. G. (2002) Spectroscopic properties of a mitochondrial cytochrome *c* with a single thioether bond to the heme prosthetic group, *Biochemistry 41*, 7811-7818.

Schellman, J. A. (1978) Solvent denaturation, *Biopolymers 17*, 1305-1322.

Wandschneider, E., Hammack, B. N., and Bowler, B. E. (2003) Evaluation of cooperative interactions between substructures of iso-1-cytochrome *c* using double mutant cycles, *Biochemistry 42*, 10659-10666.

Wang, Z., Matsuo, T., Nagao, S., and Hirota, S. (2011) Peroxidase activity enhancement of horse cytochrome *c* by dimerization, *Org. Biomol. Chem. 9*, 4766-4769.

Winklhofer K.F., Tatzelt J., and Haass, C.; The two faces of protein misfolding: gain- and loss-of-function in neurodegenerative diseases *The European Molecular Biology Organization Journal* 27(2008):336-349.

Ying T., Zhong F., Xie J., Feng., Wang Z-H., Huang Z-X., Tan X.; Evolutionary alkaline transition in human cytochrome *c Journal of Bioenergetics and Biomembranes* 41(2009):251-257.